# CoNiGa HIGH TEMPERATURE SHAPE MEMORY ALLOYS

A Thesis

by

EBUBEKIR DOGAN

Submitted to the Office of Graduate Studies of
Texas A&M University
in partial fulfillment of the requirements for the degree of

MASTER OF SCIENCE

August 2010

Major Subject: Mechanical Engineering

CoNiGa High Temperature Shape Memory Alloys

# CoNiGa HIGH TEMPERATURE SHAPE MEMORY ALLOYS

A Thesis

by

EBUBEKIR DOGAN

Submitted to the Office of Graduate Studies of
Texas A&M University
in partial fulfillment of the requirements for the degree of

MASTER OF SCIENCE

Approved by:

| | |
|---|---|
| Chair of Committee, | Ibrahim Karaman |
| Committee Members, | Raymundo Arroyave |
| | Haiyan Wang |
| Head of Department, | Dennis L. O`Neal |

August 2010

Major Subject: Mechanical Engineering

# ABSTRACT

CoNiGa High Temperature Shape Memory Alloys.

(August 2010)

Ebubekir Dogan, B.S., Bogazici University

Chair of Advisory Committee: Dr. Ibrahim Karaman

Shape memory alloys (SMAs) are an important class of smart materials that have the ability to remember a shape. Current practical uses of SMAs are limited to below 100°C which is the limit for the transformation temperatures of most commercially successful SMAs such as NiTi and Cu-based alloys. In recent years, the CoNiGa system has emerged as a new ferromagnetic shape memory alloy with some compositions exhibiting high martensitic transformation temperatures which makes CoNiGa a potential high temperature shape memory alloy (HTSMA). In this study, the microstructural evolution and martensitic transformation characteristics of CoNiGa (mainly $Co_{46}Ni_{27}Ga_{27}$ and $Co_{44}Ni_{26}Ga_{30}$ in at.%) HTSMAs were investigated in as-cast and hot-rolled conditions as a function of different heat treatments. Heat treatment conditions were selected to introduce single, two, and three phase structures, where two precipitate phases (ductile $\gamma$ and hard $\gamma'$) do not martensitically transform. Calorimetry, X-ray analysis, scanning and transmission electron microscopy, thermo-mechanical process and cycling techniques are applied to understand the structural and chemical factors influencing the thermal stability and transformation characteristics. The main

findings include improvement of ductility, most cyclically stable compositions with narrow transformation hysteresis (<40°C) and transformation temperatures in the range of 100°C to 250°C, formation of new phases and their effects, and associated compositional changes in the matrix, on the transformation temperatures and on the microstructural evolution. In addition, $M_s$ temperature depends linearly on the valence electron concentration (e/a) of the matrix, only if the Ga content is constant, and the samples with narrow transformation hysteresis demonstrate reversible martensitic transformation in constant-stress thermal cycling experiments.

To My Wife and My Parents

.

## ACKNOWLEDGEMENTS

First of all, I would like to thank my advisor, Prof. Ibrahim Karaman, who gave his endless encouragement and support to this project. He always motivated me like a coach and helped me in all aspects of this project and turned me into a researcher. He has been a good model for me and influenced me in almost every aspect of my academic life.

I would like to thank my committee member, Prof. Raymundo Arroyave, for sharing his valuable comments and suggestions about my study. I am also grateful to Prof. Haiyan Wang for being a member of my committee and a role model.

I would like to express my appreciation to Prof. Yuriy Chumlyakov for his motivation in my research and sharing with me his deep knowledge on shape memory alloys. I am also thankful to Dr. Zhipping Luo for his endless patience during long-lasting experiments. He helped me tremendously on TEM and indexing diffraction patterns.

I would like to thank my officemates, especially Can Atli and Ji Ma, who shared their experiences and helped a great deal with my study. I would also like to thank my other office mates, Burak Basaran, Erhan Akin, Fevzi Ozaydin, Nevin Ozdemir, Cengiz Yegin, James Monreo and Ruixian Zhu, who provided a great environment and support during my study. I would like to express my special thanks to Erhan, Can and Cengiz because of their good friendship not only in the office but also in my social life.

Finally, I would like to thank my parents who have loved, supported and trusted me throughout my life. I have always felt very lucky for having them. I would also like to thank my wife because of her never-ending patience and support during my graduate education. Words cannot express how much I appreciate her having postponed her career and choosing to live far away from her parents for me. Also, thanks to my brothers and sisters for their endless support throughout my life. I appreciate knowing that my family supports me and loves me unconditionally.

# TABLE OF CONTENTS

CHAPTER Page

# LIST OF FIGURES

Page

Page

Page

Page

# LIST OF TABLES

# CHAPTER I

# INTRODUCTION

## 1.1 Background

Shape memory alloys (SMAs) are a unique material class that has a different philosophy than commercial alloys such as steel and titanium alloys. Large recoverable shape change is observed as a result of cooperative motion of atoms, which is the result of diffusionless solid-solid phase transformation. The time-independent solid-solid phase transformation can be triggered by change in temperature, stress or magnetic field.

The shape memory effect (SME) is recovering of large strain as a result of martensitic transformation upon heating at austenite finish ($A_f$) temperature. The low temperature phase is called martensite and the high temperature phase is referred to as austenite. Martensitic transformation is a diffusionless phase transformation which occurs by a large shear-like deformation associated with a very short movement of atoms (less than inter atomic distance), different than long range diffusion of atoms [1-3]. The shear-like deformation is generally about 20 times more than the elastic deformation [1].

Shape memory was first observed in Au-Cd [4] and In-Ti [5] alloys in the 1950s. However, at that time, it was not called the shape memory effect. It was first realized as shape memory effect in Ti-Ni alloys, which was initially called the peculiar memory effect [6]. Conversely, SME has been also found in Cu-Al-Ni [7] alloys were initially attributed to thermoelastic transformation in Cu-Al-Ni alloys [8]. After that, basic

---

This thesis follows the style and format of *Acta Materialia.*

concepts of the SMAs, such as SME, shape memory mechanism and stress-induced martensitic transformation, have been widely investigated for Cu- based alloys [8-11]. Since making single crystals of Cu based alloys is easier than Ti-Ni alloys, first studies on SMAs were established for Cu-based alloys [1]. On the other hand, Ti-Ni alloys are the most commercial SMA because of its good workability in polycrystalline form and it has superior characteristics for application purposes.

In addition to the shape memory effect, another unique feature, superelasticity (SE), has been observed in the SMAs. SE is related to large nonlinear recoverable strain upon loading and unloading at higher temperatures [12].

**1.2 Martensitic Transformation**

The basic mechanism of the martensitic transformation is essential to understand SME and SE. Solid state transformations can be divided in two; diffusional and diffusionless (displacive) transformations [13]. Diffusional transformation includes the random movement of atoms to long distances. After the transformation chemical compositions of new formed phases are different than the matrix composition. Distance traveled by atoms is usually longer than inter atomic distance, thus the transformation requires both time and temperature [13].

In diffusionless transformation, atoms move cooperatively and the movement is short range associated with rearrangement of atoms by shear-like mechanism. As a result of the transformation a more stable crystal structure forms without any chemical compositional change. Martensitic transformation is generally classified as diffusionless transformation [13].

The high temperature structure is called the parent phase which is usually cubic, and the lower temperature phase is martensite which has a lower symmetry [12]. During martensitic transformation the interphase between the parent phase and martensite variant stays undistorted and unrotated in the sake of strain energy minimization [1]. Since martensitic transformation is a diffusionless transformation there is a one to one correspondence both in the directions and planes (habit plane) between martensite and the parent phases [12].

Figure 1.1 presents martensitic transformation schematically. The figure represents how martensitic transformation occurs as a result of military motion of the atoms. Thus, martensite transformation is also called the military transformation [12].

When martensite is heated at a certain temperature, Austenite start ($A_s$) temperature, martensite becomes unstable and the reverse transformation starts by shear-like mechanism as shown in Figure 1.1. When the temperature is above $A_f$ martensite completely transforms to the parent phase. If the temperature is lowered to martensitic start ($M_s$) temperature the transformation starts, and below martensite finish ($M_f$) temperature the parent phase completely transforms to martensite. Upon a temperature increase again then martensite transforms to the parent phase in the original orientation. Therefore, in the reversible martensitic transformation not only the crystal structure of the parent phase, but also the orientation is remembered [2].

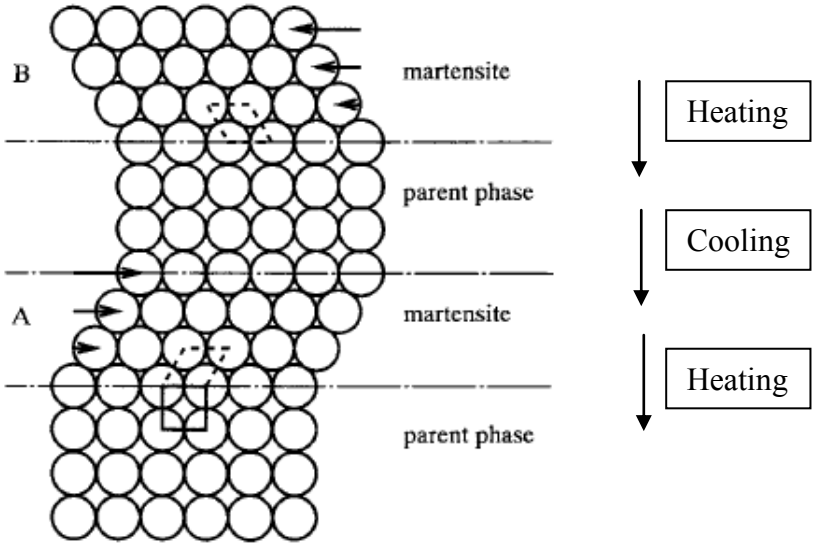


**Figure 1.1** A model of Martensitic transformation [12]

Note that, the orientations of the martensites in A and B (Fig. 1.1) are different although they have the same structure. These two orientations are called the correspondence variants of martensites [12]. Generally, there are several correspondence variants of martensites from same the parent phase [12]. The martensite variants are formed by introducing twinning which is reversible in SMAs [1].

During the transformation large strain generates around the martensite. There are two general mechanisms, slip and twinning, to reduce large strain associated with the transformation. These deformations are called the lattice invariant shear (LIS) [12, 14]. Which type of slip and twinning forms during transformation depends on the kinds of alloys. Slip is a common accommodation mechanism in many martensites which is permanent [13]. Figure 1.2 shows the lattice deformation (Fig. 1.2.a) and accommodations of strain by slip (Fig. 1.2.b) and twinning (Fig. 1.2.c) upon a

martensitic transformation. In the slip type accommodation atomic bonds are broken (Fig. 1.2.b). However, in the twinned structure all atoms stay in touch with the neighbors atoms (Fig. 1.2.b).

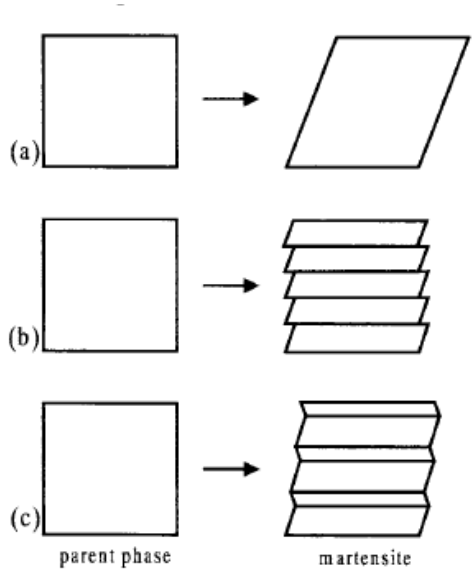


**Figure 1.2** Schematic representation of (a) the lattice deformation (shape change), (b) accommodation of strain by slip shear, (c) accommodation of strain by twinning shear upon martensitic transformation [12].

Twinning can store shape change in a reversible way but it is unable to accommodate volume change. In SMAs such as NiTi, martensite involves only shape change but in steel it undergoes both volume and shape changes [13]. Thus, martensitic transformation does not result in shape memory behavior in steel.

Martensitic transformation can be divided in two types; thermoelastic and non-thermoelastic. In thermoelastic transformation, lattice strain that is created upon transformation is stored and the stored strain causes reversibility of the austenite to

martesite. In addition, thermal hysteresis is generally low (<100°C). On the other hand, non-thermoelastic transformation involves nucleation of austenite during the reverse transformation and, thus, high thermal hysteresis (several hundred Celsius). SMAs generally show thermoelastic transformation which is associated with reversibility and low thermal hysteresis. However, some cobalt and iron base SMAs exhibit non-thermoelastic transformation having thermal hysteresis of more than hundred Celsius which is somewhat reversible [3].

Martensitic transformation is a first order transformations which includes both nucleation and growth. When martensite is formed heat is generated and there is a hysteresis during transformation that means there is a temperature range where austenite and martensite co-exist [13].

In order to transform from parent phase to martensite, the chemical free energy of the martensite should be lower than the parent phase. In addition, the difference between chemical free energies of the martensite and the austenite should be equal to non-chemical free energy, such as strain and interphase energy, in order to start transformation. Therefore, driving force is necessary to start martensitic transformation which is nonchemical free energy. In order for transformation to progress, the parent phase should be cooled to $M_s$ from the equilibrium temperature of chemical free energies of martensite and austenite ($T_0$). In the same manner, martensite should be heated to high temperatures in order to start reverse martensitic transformation ($A_s$) [14]. Figure 1.3 demonstrates how chemical free energies of the martensite and austenite change upon

temperature. The difference between chemical free energies where martensitic transformation starts, gives the non-chemical free energy.

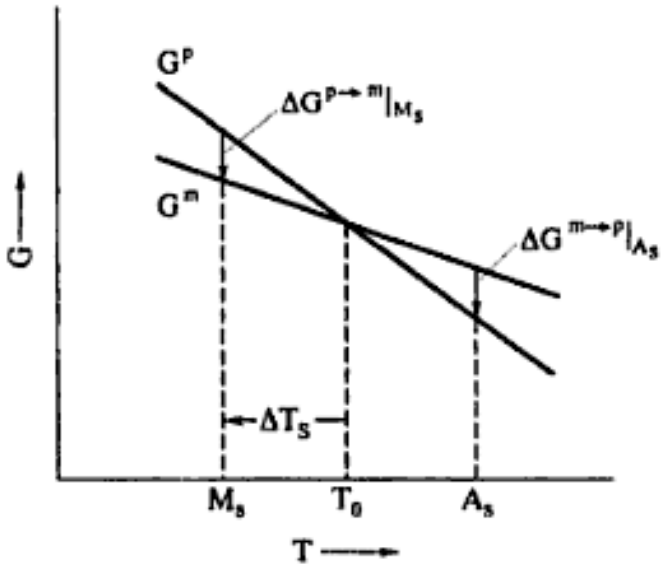


**Figure 1.3** Schematic representation of the chemical free energy changes of the martensite and austenite upon temperature change [12]. $G^M$ : Chemical free energy of martensite $G^P$: Chemical free energy of austenite

### 1.3 Shape Memory Effect

Shape memory effect can be simply defined as a phenomenon that when the material is deformed at temperatures below $A_s$, it returns to its original shape when the sample is heated at temperatures above $A_f$ [12]. The origin of the shape memory comes from reversibility of the parent phase orientation. As explained above, there is more than one possibility of the martensite formation from one parent phase, however there is only

one way for martensite to return to parent phase. Therefore, one of the requirements for shape memory is that during the transformation the parent phase orientation should be restored. In addition, martensitic transformation should have only very small volume change and during martensitic transformation, slip should not be involved. Figure 1.4 demonstrates the shape memory effect. When stress is applied and twinned martensite (A in the Fig. 1.4) is deformed, twin boundaries move from one correspondence martensite variant to another. The most favorable correspondence martensite variant is selected under the applied stress upon the detwinning mechanism (B in the Fig. 1.4). When stress is removed, elastic strain is recovered; however, a major part of the strain that is introduced by the detwinned structure remains (C in the Fig. 1.4). Since the sample temperature is under $M_f$ temperature, martensite stays as detwinned martensite. When the sample is heated at temperatures above $A_s$, twin boundaries migrate again and the original orientation of the austenite is restored (D in the Fig. 1.4). As a result, all strain introduced by reorientation and the detwinning of martensite is recovered. When the sample is cooled `self accommodated martensite` arises (E in the Fig. 1.4). The described process is called one way shape memory because recovery is only one way from detwinned martensite to austenite upon heating [1, 3].

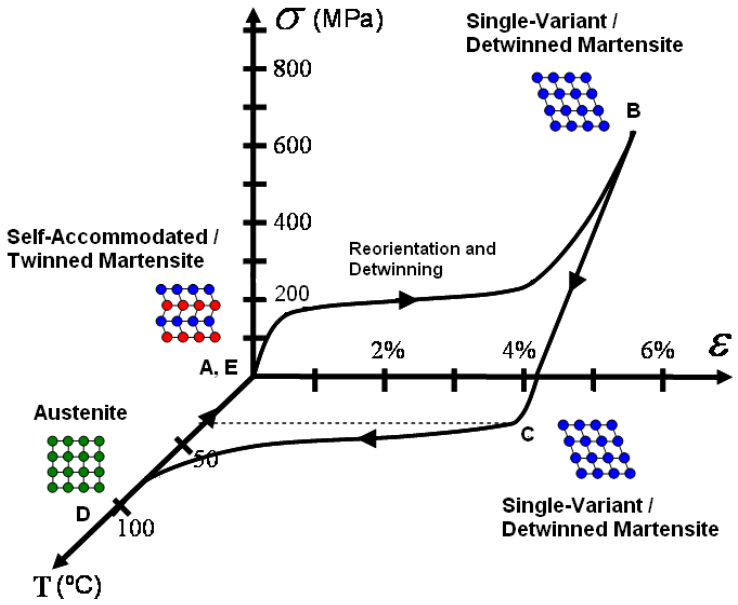


**Figure 1.4** Schematic representation of the shape memory process [3]**.**

The martensitic transformation described above is thermoelastic transformation where the transformation is crystallographically reversible. In addition, mostly the ordered alloys show thermoelastic reversible martensitic transformations. However, most of the ferrous shape memory alloys exhibit thermoelastic martensitic transformation, although their parent phases are not ordered. Reversibility of such ferrous alloys can be improved by ordered γ` precipitation in the austenite. These $L1_2$ ordered structure precipitates disperse in the matrix and strengthen the austenite, resulting in a high mobility of the interphase between the parent phase and martensite [1-2]. This phenomenon is also applicable for CoNiGa SMAs to improve shape memory effect.

### 1.4 Stress Induced Martensite and Superelasticity

The martensitic transformation can happen by three types of stimulus such as heat, stress and magnetic field. It was explained before that at temperatures above $M_s$ martensite structure is stable, and above $A_s$ parent phase is more stable. However, above $M_s$ martensite can also be more stable than the parent phase under stress. Stress induced martensite (SIM) can be introduced by applying stress at constant temperatures above $A_f$ as a result of parent phase transformation to martensite. The driving force for transformation is, now stress, as opposed to heat. Another type of shape memory, SE, which is temperature independent and has a driving force of applied stress [2, 13]. Thus, it can be stated that a decrease in temperature can have the same function with an increase in stress in terms of martensite stabilization [13].

As a result of stress induced martensite there is only one single variant martensite that occurs as opposed to self accommodated martensite upon cooling. SIM causes overall shape change, however self accommodated martesite does not because of many martensite variants formation. Strain produced upon different martensite variants formations cancel out each other and the overall strain goes to zero [13].

Figure 1.5 displays stress-strain curve of regular SMAs showing superelasticity. When the parent phase is deformed to stress levels above elastic region, the parent phase transforms to single variant martensite/detwinned martensite. After the elastic region of the parent phase there is a plateau region, inelastic region, which is associated with phase transformation. After the inelastic region martensite deforms elastically where stress increases suddenly. When the stress is removed martensite transforms to original

orientation of the parent phase and overall shape change is recovered. There is a stress hysteresis shown in the figure that is indicator of strain energy dissipation during superelastic behavior.

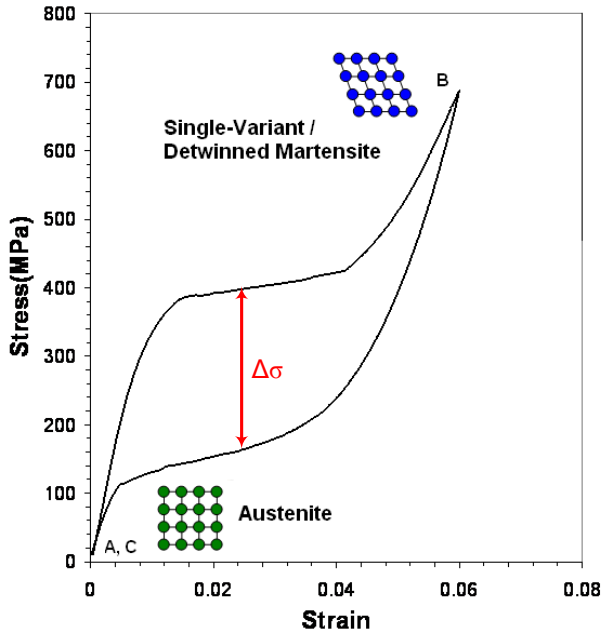


**Figure 1.5** Demonstration of the superelasticity on stress-strain curve. (A) austenite, (B) single variant martensite and (C) same orientation austenite with (A) [3].

As it is obvious in the figure, a stress limit is required for SIM. The stress limit depends on the temperature at which the sample is deformed superelastically. Since full recoverable SE is reversible, slip does not involve in the deformation. Thus, stress required to SIM should be below the critical stress for the slip.

Figure 1.6 represents schematic diagram of the regions where SMAs show SME and SE. There are two straight lines with negative slopes showing the critical stress

levels of the slip with respect to temperatures. In other words, the critical stress for slip decreases when the temperature increases. On the other hand, the critical stress for SIM increases with temperature. One of the negative slope lines represents low level of the critical stress for slip. As seen from the graph, if the critical stress for slip is low, material does not show superelastic behavior. Since critical stress for slip is lower than the critical stress for SIM at temperatures above $A_f$, slip happens always prior to SIM which is associated with SE. Thus, high critical stress for slip is essential for SME and SE. In order to improve superelasticity of the SMAs, material can be strengthened by precipitation hardening which increases the critical stress for slip [2].

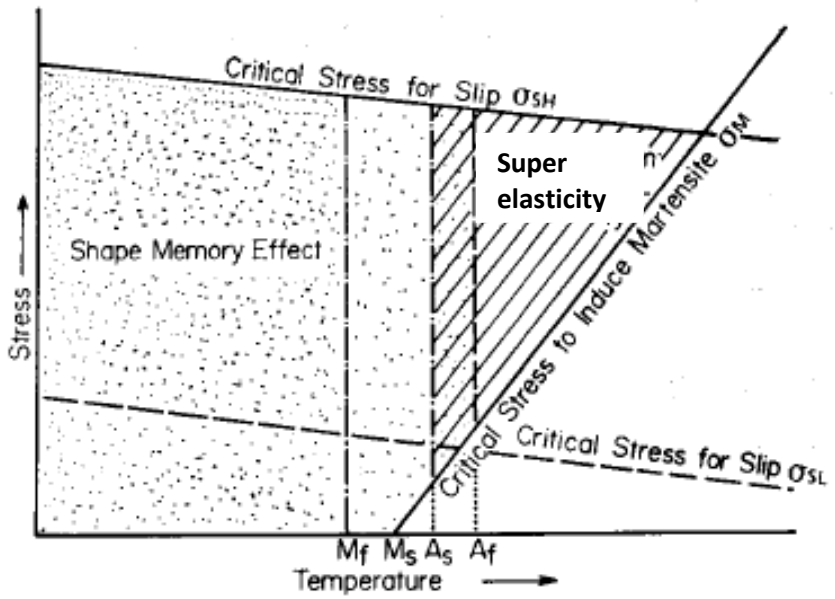


**Figure 1.6** Schematic diagram showing the regions of the shape memory effect and superelasticity in the temperature-stress coordinates. $\sigma_M$: The critical stress for SIM, $\sigma_{SM}$: The high critical stress for slip, $\sigma_{SL}$: The low critical stress for slip [1].

### 1.5 Shape Memory Applications

Since the discovery of the SMAs there are tremendous various applications have been suggested because of unique properties of the SMAs. Since SMAs have impressive physical properties as opposed to commercial alloys, designers have produced impressive ideas and some of them are used in different areas. Product diversity can be listed as medical wires, eyeglasses frames, pipe couplings, electronic connectors, sensors and actuators [12-13].

SMAs applications can be classified into four main catagories: free recovery, constrained recovery, work production and superelasticity [13]. Using basically only the SME involves free recovery. Free recovery means that without any constrains the material recovers its original shape upon heating. Constrained recovery can be defined as preventing the recovery; thus stress is produced upon transfromation. Pipe coupling can be classified as constrained recovery type of applications. Work production applications are under constant stress, where material transforms upon thermal cycling. Therefore, material does work by transforming. Actuators can be considered this type of applications. Lastly, SE can be involved in applications requiring potential energy storage. At constant temperature it is possible to store energy 40 times larger than ordinary steel spring in some NiTi SMAs using SE [1].

### 1.6 High Temperature Shape Memory Alloys

Current practical uses of shape memory alloys (SMAs) are limited to below 100°C which is the limit for the transformation temperatures of the most commercially successful SMAs such as NiTi and Cu-based alloys. High temperature SMAs

(HTSMAs) can be classified as SMAs having $M_s$ of above 100°C [3, 15-16]. Since below this temperature the diffusion process is difficult to take place, reversibility of the transformation is easy [15]. However at high temperatures diffusion controlled mechanisms are activated easily and the reversibility of the martensitic transformation is difficult.

Some of the challenges for HTSMAs are listed as; stabilization of the martensite at high temperatures before reverse transformation occurs, decomposition of the martensite or the parent phase, recrystallization, creep, oxidation etc. One of the main problem for HTSMAs is low critical stress for slip at high temperatures. The negative slope is shown in the Figure 1.6 demonstrates how the critical stress for slip decreases upon temperature increase. At high temperatures slip occurs more easily than SIM. In this regard, HTSMAs has many obstacles to perform like functionally stable and reliable low temperature SMAs, such as NiTi [15-16].

Recently, automotive, aerospace, and public utility industries have become interested in high temperature SMAs (HTSMAs) with transformation temperatures between 100 and 250 °C [3, 15]. Some of the known HTSMAs with transformation temperatures in this range include NiTiX, where X is Pd, Au, Pt, Hf and Zr [3] , CuAlNi(Zn) [16] , NiMnGa [17-18] and NiAl [16] alloys. Among NiTiX alloys, NiTiPd, NiTiPt, NiTiAu alloys are most promising HTSMAs due to their relatively good workability, low transformation hysteresis and dimensional stability, however, they are very expensive because of Pt, Pd, and Au additions [16, 19-20]. NiAl alloys, have poor low temperature ductility and fracture toughness [21]. In addition, $Ni_5Al_3$ phase

formation at high temperatures prevents martensite reversibility [21-22]. Cu-based alloys suffer from chemical and thermal stabilities because of the tendency for compositional decomposition at high temperatures [23-24]. NiMnGa alloys are prone to intergranular fracture [3]. NiTi (Hf,Zr) alloys demonstrate high transformation hysteresis, thermal cyclic degradation and dimensional instability [16, 25-27].

Thermal stability upon cycling through reversible martensitic transformation either thermally or thermo-mechanically is one of the critical features that HTSMAs should posses in order to be utilized in practical applications. Therefore, there is a pressing need for the development of relatively inexpensive HTSMAs with reasonable thermal and chemical stability. In addition HTSMAs must have functional stability and superior mechanical properties. Dislocation and grain boundary mediated plasticity is the most basic problem for HTSMAs that manifests itself as the large irrecoverable strain in the SME and as the lack of SE.

**1.7 Motivation**

In recent years, CoNiAl [28-33] and CoNiGa [34-43] systems have emerged as new ferromagnetic shape memory alloy systems, possibly alternatives to NiMnGa alloys. CoNiGa usually has higher reported $M_s$ temperatures than CoNiAl and show SE at high temperatures [35-36, 44]. In addition, CoNiGa system has a better control of ductile second phase formation and thus, ductility, the wide range of stability of the B2-β phase in the Ni-Ga and Co-Ga binaries, and the existence of a β+γ equilibrium in the Co and Ni-rich regions [45].

Most of the works on CoNiGa alloys up to date have focused on their magnetic properties [38-39, 42, 46], shape memory and SE responses, however, studies are mainly on single crystalline alloys and alloys with $M_s$ temperatures less than 100°C [34-37, 47]. Dadda *et al.* [35-37] demonstrated excellent low temperature shape memory and SE response in single crystalline CoNiGa alloys. It also has been shown that single crystalline $Co_{49}Ni_{21}Ga_{30}$ alloy exhibits good cyclic stability and SE up to 450 °C along the [100] orientation under compression [36-37], much higher than highest temperature (230 °C) at which SE has been reported to date [10, 47]. However, information on the shape memory and SE response of CoNiGa SMAs in polycrystalline form is very limited, and there is only one reported work on the shape memory response of high temperature compositions [48].

The main reason for the lack of extensive studies on polycrystalline CoNiGa HTSMAs, despite their potential as relatively inexpensive alternatives to NiTi(Pd, Pt, Au) HTSMAs, is the brittleness of polycrystals stemming from the lack of sufficient numbers of deformation systems, and thus, the intergranular fracture. The ductility of brittle single phase CoNiGa polycrystals can be improved by utilizing ductile Co-rich γ (disordered A1 type fcc) second phase [40]. Prusik *et al.* [49] investigated the effects of the γ phase on ductility of CoNiGa SMAs. They reported that increase in γ phase volume fraction significantly improves plasticity of CoNiGa alloys [49]. Therefore, the precipitation of ductile γ phase can make polycrystalline CoNiGa SMAs tougher and workable.

Engineering of hard, coherent, non-transforming nanoprecipitates under constrained aging (i.e. aging under stress leading to the selection of a single precipitate variant) significantly improves cyclic transformation stability and functional fatigue response of Ni-rich NiTi SMAs [50-51]. Similar effects of aligned coherent nanoprecipitates (γ') are expected in CoNiGa which should be beneficial especially for cyclic transformation stability and against creep and plasticity.

To date the effect of γ phase on ductility has been widely investigated [49, 52], on the other hand, the information related to its effects on martensitic transformation characteristics is scarce in the literature. In addition, ordered γ' phase ($L1_2$ type fcc) precipitates have been found in CoNiGa systems [43, 53], however, their role on mechanical properties and reversible martensitic transformation has not been studied in high transformation temperature compositions and polycrystals.

In the SMA literature, $M_s$ temperature vs. valence electron concentration (e/a) relationship is commonly used to better illustrate the compositional dependence of $M_s$ temperature. In NiMnGa, NiMnIn, NiMnSn, and NiMnSb systems $M_s$ dependency on e/a ratio is well established [54-56], and there is an excellent linear correlation between $M_s$ and e/a ratio, the slope of which is a function of a groups [56]. During the last decade, few researchers have also looked for a similar relationship in CoNiGa SMAs [38, 41, 44, 57]. A good linear dependency of $M_s$ temperature on e/a ratio was shown by Creciunescu *et al.* [57] using the nominal compositions of their alloys. However, whether the alloys had a single or multiple phases was not specified, and if they have multiple phases, the composition of the B2 matrix was not specified. Oikawa *et al.* [41]

showed a linear dependence between $M_s$ temperature and e/a ratio only for single phase CoNiGa alloys, however, the trend lines were completely different for 32 at.% Ga and 30 at.% Ga alloy series. The reason for a strong influence of Ga on the Ms temperature vs. e/a ratio is surprising since this is not the case in NiMnGa SMAs[56] and Oikawa *et al.* [41] did not provide any insight for this difference.

A simple linear relationship between $M_s$ temperature and e/a ratio provides the possibility of a wide transformation temperature range by simply controlling the composition of β single phase alloys or the matrix composition of multiphase CoNiGa SMAs via simple heat treatments [41, 44]. Liu *et al.* [44] showed the change in $M_s$ temperature with different heat treatments in the range of 50 to 250 °C on a two phase (β-γ) $Co_{46}Ni_{27}Ga_{27}$ alloy.

Electron concentration (e/a) of the matrix has been widely studied and is an important and effective parameter in alloy design. In addition, how the presence of γ and γ` influences this relationship has not been studied. The compositional changes upon a precipitation would definitely change the $M_s$ temperature through changing e/a ratio, however, it is not known whether any additional factors would play a role in the transformation temperatures of CoNiGa HTSMAs, such as the type, size volume fraction, and coherency of precipitates. The present work addresses some of these issues in CoNiGa HTSMAs.

In summary, CoNiGa SMAs are promising low cost alternatives to NiTi(Pd, Pt, Au) HTSMAs due to the availability of high transformation temperature compositions, good SE and cyclic stability in single crystals at elevated temperatures, the formation of

ductile γ phase and its positive influence on the ductility of otherwise brittle alloys, and the formation of ordered γ` precipitates with the potential of enhancing cyclic reversibility of martensitic transformation. Thus, a systematic investigation on compositions of the CoNiGa SMA system, with the high transformation temperatures and their shape memory characteristics, is needed in order to realize their potentials as HTSMAs.

In the present study, several polycrystalline CoNiGa alloys were investigated for above purposes. $Co_{46}Ni_{27}Ga_{27}$ and $Co_{44}Ni_{26}Ga_{30}$ alloys (at. %.) are mainly studied alloys in terms of SME and martensitic transformation characteristics. These compositions were selected because of their high $M_s$ temperatures, 250 °C and 170 °C respectively [41, 44]. In addition, several CoNiGa alloys with expected $M_s$ between 50-150 °C have been studied to characterize how transformation temperatures change with the compositional change. Some of the CoNiGa alloys are selected from different regions of the predicted ternary phase diagrams to validate predictions experimentally although they are not SMAs.

Selected heat treatments were conducted in as-cast and hot rolled conditions to investigate microstructural evolution and the martensitic transformation behavior. In particular, the change in transformation temperatures was revealed and their thermal cyclic stability was evaluated. Microstructural characterization using optical microscopy (OM), Scanning Electron Microscopy (SEM) with Wavelength Dispersive Spectroscopy (WDS) and Transmission Electron Microscopy (TEM) with in-situ heating stage was conducted to understand the structural and chemical factors influencing the thermal

stability. In addition, ductility and shape memory response of hot rolled $Co_{46}Ni_{27}Ga_{27}$ alloy was investigated to demonstrate the effect of γ phase on ductility and to determine transformation strain level of this polycrystalline alloy.

# CHAPTER II

# EXPERIMENTAL TECHNIQUES

Different CoNiGa alloys were prepared by vacuum arc-melting of 99.9% Co, 99.95% Ni and 99.999% Ga. Usually arc-melted buttons are homogenized at temperatures about 50-100°C below of the predicted melting temperatures by thermodynamic models of our colleagues [58]. Note that a complete ternary phase diagram is not available. There are a few ternary phase diagrams in the literature [41, 43, 59]. Most of them have limited information and are not complete.

Mainly worked two alloys with nominal compositions of $Co_{46}Ni_{27}Ga_{27}$ and $Co_{44}Ni_{26}Ga_{30}$ (in at.%) were also prepared by vacuum arc-melting of 99.9% Co, 99.95% Ni and 99.999% Ga. Small pieces were cut, homogenized at 1200 °C for 4hrs in argon followed by water quenching, and annealed at different temperatures to investigate the formation of γ phase. The remaining $Co_{46}Ni_{27}Ga_{27}$ button was initially homogenized at 1150°C for 8 hrs followed by 1100 °C heat treatment for 24 hrs in and air cooled (called as initial-HT). This heat treatment was selected to form a high volume fraction of γ phase according to [44]. The initial-HT button was then hot-rolled in a steel can at 900 °C to 40% thickness reduction.

The microstructures of the samples were examined using a digital Keyence VH-Z100 optical microscope (OM) and a Cameca SX50 scanning electron microscope (SEM). The local chemical analysis of the phases was performed in the SEM equipped with four wavelength dispersive X-Ray spectrometers (WDS). The OM samples were etched in the 50% hydrochloric acid, 33% ethanol, 8.5% copper sulfate and 8.5% water

solution .The crystal structure of different phases were determined using a Bruker-AXS D8 X-ray diffractometer (XRD) with $CuK_{\alpha}$ (0.15406 nm) radiation. Stress free transformation temperatures were determined using a Perkin-Elmer Pyris I differential scanning calorimeter (DSC) at a heating/cooling rate of 30°C/min. Transmission electron microscopy (TEM) analysis was conducted using a JEOL 2010 microscope operated at an accelerating voltage of 200kV. TEM foils were prepared from the bulk samples by mechanically grinding down to 100μm, punching out 3mm diameter disks from the thin foils and subsequently ion milling under 3kV and 5mA. In-situ heating experiments were conducted in the TEM to monitor the microstructural changes during heating and cooling across the phase transformation temperatures.

Flat dog-bone shaped tension specimens with gage dimensions of 8 mm x 3 mm x 1.5 mm were cut from the hot rolled button using wire electrical discharge machining (EDM). Tension experiments were performed in a servo-hydraulic MTS test frame. An MTS high temperature extensometer with a gage length of 12.7 mm was used to measure the axial strain. The extensometer had a pair of ceramic rods, 3.5 mm in diameter with V-chisel ends exerting a 300 g force per rod on the sample. Constant-stress thermal cycling response of the hot rolled $Co_{46}Ni_{27}Ga_{27}$ samples were examined under incrementally increasing tensile stress levels. These experiments were conducted along both rolling and transverse directions. The constant stress levels used were 50, 150, 200, 250, and 300 MPas with temperature cycling range of 50°C to 250°C, decided upon the DSC results. The goal was to reveal transformation strain levels, transformation temperatures and hysteresis as a function of the bias stress level. Rectangular

compression samples (4 mm x 4 mm x 8 mm) were cut from the hot rolled button. The compression experiments were conducted using an electromechanical MTS testing system. A miniature MTS extensometer (3 mm gage) was used to measure the axial strain.

# CHAPTER III

# EXPERIMENTAL RESULTS

All experimental results of the polycrystalline CoNiGa HTSMAs studied are listed in Table 3.1. Table includes different heat treatments, phase compositions, volume fraction of γ phase, e/a ratio of the matrix, and transformation temperatures of these HTSMAs. The matrix compositions of the multiphase alloys are measured to calculate the e/a ratio of the matrix. The volume fraction of γ phase is measured using an image processing software. Increase of γ phase volume fraction significantly improves the formability of CoNiGa alloys [49].

## 3.1 Microstructural Evolution

Figure 3.1 displays optical microscopy and SEM BSE images of a few CoNiGa alloys listed in Table 3.1. Note that these samples were homogenized at 1200°C for 4 hrs and water quenched. Optical micrograph of the single phase $Co_{44}Ni_{26}Ga_{30}$ alloys having

**Table 3.1.** All experiment results of CoNiGa alloys showing list of different heat treatments, phase compositions, volume fraction of γ phase, the e/a ratio of the matrix, transformation temperatures. Initial-HT: 1150°C 8 hrs + 1100 °C for 24hrs + Air Cooling. WQ: Water Quenched, AC: Air Cooled, $M_f$: Martensite finish temperature, $M_s$: Martensite start temperature, $A_s$: Austenite start temperature, $A_f$: Austenite finish temperature, ΔT: $A_f - M_s$, NM: Not measured.

| Nominal Composition (at. %) | Heat Treatment | Matrix(B2) Composition | | | γ phase Composition | | | γ phase Volume Fraction (%)(±2) | e/a of Matrix (B2) | Mf (°C) | Ms (°C) | As (°C) | Af (°C) | ΔT (°C) |
|---|---|---|---|---|---|---|---|---|---|---|---|---|---|---|
| | | Co | Ni | Ga | Co | Ni | Ga | | | | | | | |
| **Co5Ni62Ga33** | 1127 °C 24hrs WQ | 5.33 ±0.06 | 61.96 ±0.13 | 32.72 ±0.08 | - | - | - | 0 | 7.657 | NM | NM | NM | NM | NM |
| **Co15Ni80Ga5** | 1200 °C 4 hrs WQ | | | | | | | 100 | 0 | - | - | - | - | - |
| **Co20Ni65Ga15** | 1127 °C 24hrs WQ | - | - | - | | | | 100 | 0 | - | - | - | - | - |
| **Co30Ni45Ga25** | 1127 °C 24hrs WQ | 24.44 ±0.11 | 46.50 ±0.12 | 29.07 ±0.01 | 35.52 ±0.10 | 44.40 ±0.04 | 20.08 ±0.05 | 50 | 7.721 | NM | NM | NM | NM | NM |
| **Co44Ni26Ga30** | As-Cast | 44.48 ±0.27 | 26.30 ±0.21 | 29.22 ±0.21 | - | - | - | 0 | 7.46 | 141 | 174 | 191 | 222 | 48 |
| **Co44Ni26Ga30** | 1200 °C 4 hrs WQ | 44 | 26 | 30 | - | - | - | 0 | 7.46 | 147 | 178 | 182 | 210 | 32 |
| **Co44Ni26Ga30** | 1200 °C 4 hrs WQ<br>1000°C 24 hrs WQ | NM | NM | NM | NM | NM | NM | 4 | NM | NM | NM | NM | NM | NM |
| **Co44Ni26Ga30** | 1200 °C 4 hrs WQ<br>950°C 24 hrs WQ | NM | NM | NM | NM | NM | NM | 5 | NM | NM | NM | NM | NM | NM |
| **Co44Ni26Ga30** | 1200 °C 4 hrs AC<br>900 °C 24 hrs AC | NM | NM | NM | NM | NM | NM | 5 | NM | 107 | 119 | 131 | 158 | 39 |
| **Co46Ni24Ga30** | 1200 °C 4 hrs AC | 48.13 ±0.36 | 23.47 ±0.41 | 28.40 ±0.26 | 59.36 ±0.13 | 20.55 ±0.14 | 20.08 ±0.02 | 4 | 7.531 | 98 | 111 | 129 | 144 | 33 |
| **Co46Ni27Ga27** | 1200 °C 4hrs WQ | 42.67 ±0.08 | 29.22 ±0.16 | 28.11 ±0.23 | 53.90 ±0.05 | 26.15 ±0.06 | 19.96 ±0.10 | 13 | 7.606 | 294 | 318 | 461 | 494 | 176 |
| **Co46Ni27Ga27** | 1200 °C 4 hrs WQ<br>1100°C 24 hrs WQ | NM | NM | NM | NM | NM | NM | 13 | NM | NM | NM | NM | NM | NM |
| **Co46Ni27Ga27** | 1200 °C 4 hrs WQ<br>1000°C 24 hrs WQ | NM | NM | NM | NM | NM | NM | 14 | NM | NM | NM | NM | NM | NM |
| **Co46Ni27Ga27** | 1200 °C 4 hrs WQ<br>900 °C 24 hrs WQ | NM | NM | NM | NM | NM | NM | 15 | NM | NM | NM | NM | NM | NM |
| **Co46Ni27Ga27** | Initial-HT | 42.42 ±0.2 | 28.49 ±0.09 | 29.09 ±0.19 | 56.14 ±0.23 | 24.45 ±0.11 | 19.40 ±0.14 | 28 | 7.54 | 214 | 243 | 392 | 434 | 191 |
| **Co46Ni27Ga27** | Initial-HT<br>1150°C 24 hrs WQ | 42.88 ±0.13 | 28.16 ±0.08 | 28.96 ±0.14 | 55.10 ±0.12 | 25.13 ±0.38 | 19.76 ±0.32 | 28 | 7.54 | 191 | 233 | 417 | 453 | 220 |

**Table 3.1** Continued

| Nominal Composition (at. %) | Heat Treatment | Matrix(B2) Composition | | | γ phase Composition | | | γ phase Volume Fraction (%)(±2) | e/a of Matrix (B2) | Mf (°C) | Ms (°C) | As (°C) | Af (°C) | ΔT (°C) |
|---|---|---|---|---|---|---|---|---|---|---|---|---|---|---|
| **Co46Ni27Ga27** | Initial-HT<br>1200 °C 4 hrs WQ | NM | NM | NM | NM | NM | NM | 25 | NM | 205 | 236 | 418 | 460 | 224 |
| **Co46Ni27Ga27** | Initial-HT<br>1200°C 24 hrs WQ | 43.65<br>±0.11 | 27.92<br>±0.03 | 28.42<br>±0.10 | 54.75<br>±0.29 | 24.93<br>±0.17 | 20.33<br>±0.24 | 25 | 7.57 | 200 | 247 | 442 | 472 | 225 |
| **Co46Ni27Ga27** | Initial-HT<br>900 °C Hot rolled | 40.30<br>±0.2 | 29.10<br>±0.2 | 30.60<br>±0.2 | 56.40<br>±0.1 | 24.70<br>±0.1 | 18.90<br>±0.1 | 30 | 7.45 | 133 | 172 | 156 | 210 | 38 |
| | | | | | **γ'<br>60.70<br>±0.2** | **22.20<br>±0.1** | **17.30<br>±0.1** | 4 | | | | | | |
| **Co46Ni27Ga27** | Initial-HT<br>900 °C Hot rolled<br>1000 °C 1 hrs WQ | 41.76<br>±0.07 | 28.98<br>±0.07 | 29.27<br>±0.12 | 57.38<br>±0.30 | 24.02<br>±0.31 | 18.60<br>±0.11 | 30 | 7.534 | 200 | 231 | 350 | 420 | 187 |
| **Co46Ni27Ga27** | Initial-HT<br>1200 °C 24 hr WQ<br>1200 °C 6Days WQ | NM | NM | NM | NM | NM | NM | 3 | NM | 160 | 174 | 399 | 415 | 241 |
| **Co46Ni27Ga27** | Initial-HT<br>900 °C Hot rolled<br>1200 °C 6Days WQ | 43.40<br>±0.1 | 28.50<br>±0.1 | 28.40<br>±0.1 | 54.10<br>±0.1 | 25.70<br>±0.1 | 20.30<br>±0.1 | 27-45<br>Not homogeneous | 7.61 | 264 | 281 | 444 | 469 | 188 |
| **Co46Ni27Ga27** | 1225 °C | Liquid | | | | | | | | | | | | |
| **Co49Ni22.5Ga28.5** | 1200 °C 4 hrs WQ | 48.65<br>±0.13 | 22.99<br>±0.15 | 28.36<br>±0.13 | 59.80<br>±0.04 | 20.02<br>±0.29 | 20.19<br>±0.33 | 3(±1) | 7.528 | 57 | 75 | 91 | 121 | 46 |
| **Co49.5Ni22Ga28.5** | 1200 °C 4 hrs WQ | 47.06<br>±0.34 | 23.78<br>±0.20 | 29.16<br>±0.21 | - | - | - | 0 | 7.488 | 27 | 70 | 85 | 102 | 32 |
| **Co49.5Ni21Ga29.5** | 1200 °C 4 hrs WQ | 48.18<br>±0.20 | 22.05<br>±0.14 | 29.76<br>±0.21 | - | - | - | 0 | 7.434 | 7.5 | 16.5 | 29 | 40 | 23.5 |
| **Co50Ni21Ga29** | 1200 °C 4 hrs WQ | 50.08<br>±0.06 | 21.61<br>±0.06 | 28.31<br>±0.08 | - | - | - | 0 | 7.5175 | 61 | 85 | 82 | 118 | 33 |
| **Co50.5Ni21Ga28.5** | 1200 °C 4 hrs WQ | 49.58<br>±0.29 | 21.89<br>±0.18 | 28.53<br>±0.33 | - | - | - | 0 | 7.507 | 43 | 55 | 65 | 80 | 25 |
| **Co60Ni10Ga30** | 1027°C 24hrs WQ | 58.63<br>±0.14 | 10.69<br>±0.11 | 30.68<br>±0.08 | - | - | - | | 7.30 | | | | | |
| **Co80Ni15Ga30** | 1200 °C 4 hrs WQ | - | - | - | | | | 100 | 0 | | | | | |

grain size of >100μm and small cracks along grain boundaries is presented in Figure. 3.1.a. Figures 3.1.b and 3.1.c show optical micrograph of the two phase $Co_{46}Ni_{24}Ga_{30}$ and $Co_{46}Ni_{27}Ga_{27}$ alloys, respectively, having small γ precipitates in the matrix. $Co_{46}Ni_{27}Ga_{27}$ and $Co_{46}Ni_{27}Ga_{27}$ SMAs have 13% (±2) and 4% (±2) γ phase volume fraction after heat treatment at 1200°C for 4 hrs and water quenching respectively. The SEM BSE image of $Co_{49}Ni_{22.5}Ga_{28.5}$ alloy which has small γ precipitates can be seen in Figure 3.1.d. Figures 3.1.e-g show the SEM BSE images of the single phase $Co_{49.5}Ni_{21}Ga_{29.5}$, $Co_{50}Ni_{21}Ga_{29}$ and $Co_{50.5}Ni_{21}Ga_{28.5}$ alloys, respectively. Grain size of these alloys are again on the order of >100 μm.

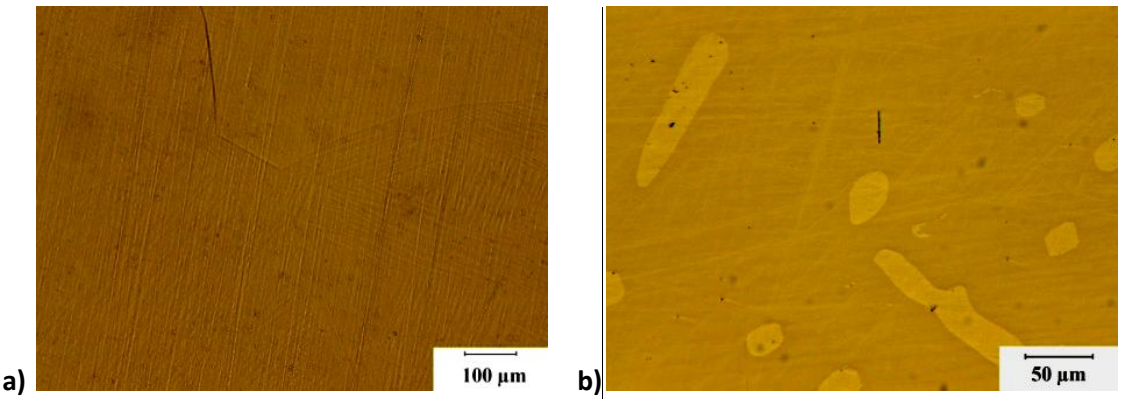


**Figure 3.1** Optical micrographs and SEM BSE images of CoNiGa polycrystalline samples after homogenization at 1200 °C for 4 hrs followed by water quenching: (a) $Co_{44}Ni_{26}Ga_{30}$, (b) $Co_{46}Ni_{24}Ga_{30}$, (c) $Co_{46}Ni_{27}Ga_{27}$, (d) $Co_{49}Ni_{22.5}Ga_{28.5}$, (e) $Co_{49.5}Ni_{21}Ga_{29.5}$, (f) $Co_{50}Ni_{21}Ga_{29}$, (g) $Co_{50.5}Ni_{21}Ga_{28.5}$.

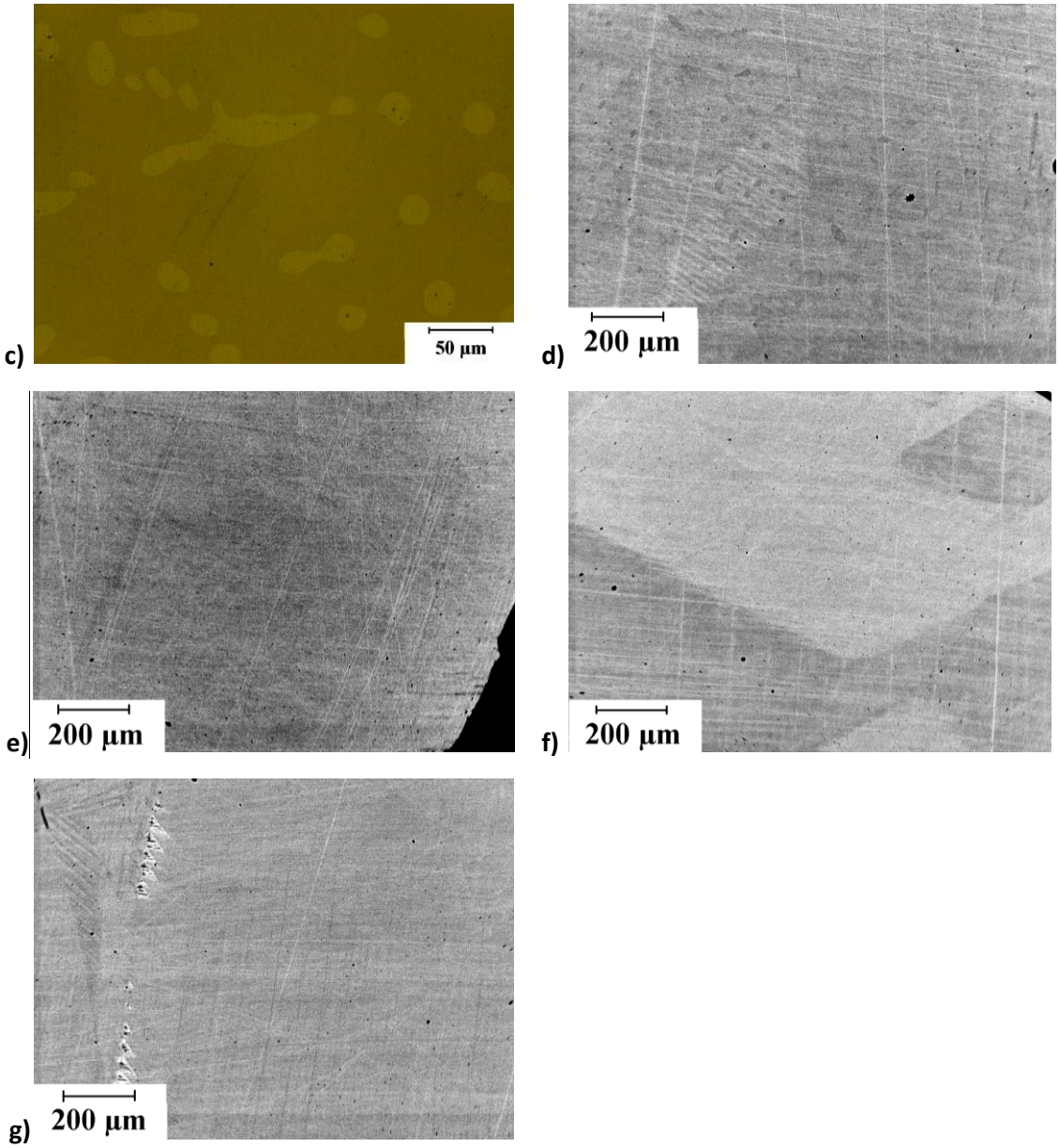


**Figure 3.1** Continued

Figure 3.2.a represents OM image of $Co_{46}Ni_{27}Ga_{27}$ after initial-HT. The sample consists of martensite and γ phase with hardness values of 236 HV and 293 HV, respectively, indicating the soft nature of the γ phase. γ phase volume fraction is

determined to be 28 % (±2). Figure 3.2.b presents the microstructure of the sample hot rolled at 900°C after the initial-HT. After the hot rolling process, new rod like γ` precipitates formed in the matrix [43]. At 900°C, it is not expected to form γ` phase according to the reported CoNiGa phase diagrams [43-44]. It forms because of very slow cooling after the hot rolling process [43]. γ` precipitates can also be a result of that ordering process in the small γ phase particles that may have formed at 900°C, during the slow cooling in the steel can similar to what was observed in NiMnGa HTSMAs [60]. This latter mechanism is supported by the TEM results which will be presented below. As a result of small γ particles which were ordered to form γ', the composition of the matrix should change, the amount of which is determined using WDS analysis (Table 3.1). As shown in the table , after the hot rolling and slow cooling, the composition and volume fraction of the initial bulky γ phase did not significantly change indicating that β→γ' transformation must have occurred. This compositional change caused a decrease in the $M_s$ temperature and e/a ratio of the matrix.

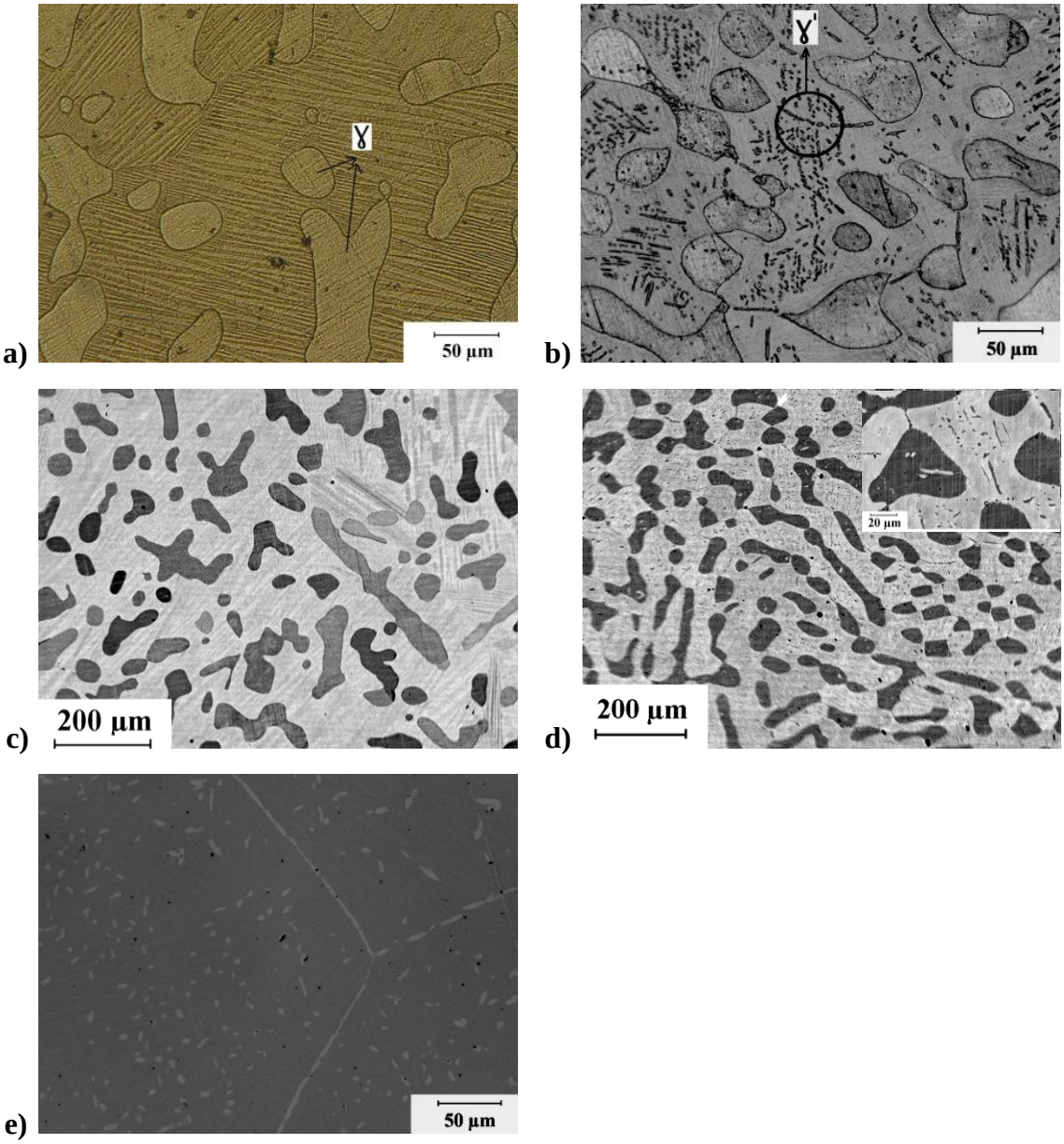


**Figure 3.2**. Optical micrographs of $Co_{46}Ni_{27}Ga_{27}$ and $Co_{44}Ni_{26}Ga_{30}$ polycrystalline samples after different thermo-mechanical treatments indicating the evolution of second and third phase particles. (a) $Co_{46}Ni_{27}Ga_{27}$ after initial-HT (1150 °C for 8hrs furnace cooling + 1100 °C 24 hrs air cooling) heat treatment. (b) the sample in (a) is hot rolled at 900°C to 40% thickness reduction. (c) and (d) SEM BSE images of the samples in (a) and (b) respectively. (f) the homogenized $Co_{44}Ni_{26}Ga_{30}$ sample heat treated at 900°C 24 hrs followed by air cooling.

After hot rolling, new small β precipitates occurred in the γ phase region, the size of the ductile γ phase particles became smaller and elongated as it can be seen clearly in the BSE images shown in Figure 3.2.c and 3.2.d, before and after hot rolling, respectively. In addition, the change in the shape and size of the γ regions indicates that the γ phase particles are heavily deformed which can only occur if the β matrix also deforms significantly during hot rolling. Since there is not a well-defined alignment of γ phase particles, for example along the rolling direction, grain boundary sliding and other diffusional mechanisms should have played a significant role in the deformation of β phase in addition to dislocation mediated mechanism.

Figure 3.2.e is the optical micrograph of the same sample shown in Figure 3.1.a after additional heat treatment at 900°C for 24 hrs. γ phase formation about 6 % is obvious after the latter heat treatment. The γ phase volume fraction didn`t change notably when the single phase sample is heat treated above 900°C or more than 24 hrs at 900°C (the results are not shown). There is a smaller size and less volume fraction γ phase formation in $Co_{44}Ni_{26}Ga_{30}$ alloy (6%) than $Co_{46}Ni_{27}Ga_{27}$ (30%) alloy. The sample heat treated at 900°C for 24 hrs, having the largest volume fraction of γ phase in this composition, was not possible to hot roll above 10% thickness reduction at 900°C, due to the lower volume fraction of γ phase compared to the $Co_{46}Ni_{27}Ga_{27}$ samples.

There is a strong tendency for grain boundary decoration observed in $Co_{44}Ni_{26}Ga_{30}$ alloy (Fig. 3.2.e). This can be favorable for polycrystalline CoNiGa SMAs since the intergranular fracture is a major problem for these alloys, grain boundary decoration of ductile γ phase is expected to improve the ductility without affecting the

shape memory response. However, formation of the ductile γ phase at grain interiors can negatively change the shape memory response of transformable matrix.

### 3.2 Structural Analysis

Figure 3.3 presents the X-ray diffraction pattern of the $Co_{46}Ni_{27}Ga_{27}$ samples after heat treated at 1200 °C for 4 hrs and hot rolling at 900 °C. Crystal structures of the phases present are determined to be $L1_0$ for martensite, A1 for γ phase (disordered fcc), and $L1_2$ for γ` phase (ordered fcc) which matches with what is reported in the literature [40-41, 43, 46] and with the TEM results shown later. The heat treated at 1200°C for 4 hrs sample has two phase microstructure having $L1_0$ matrix and γ phase.

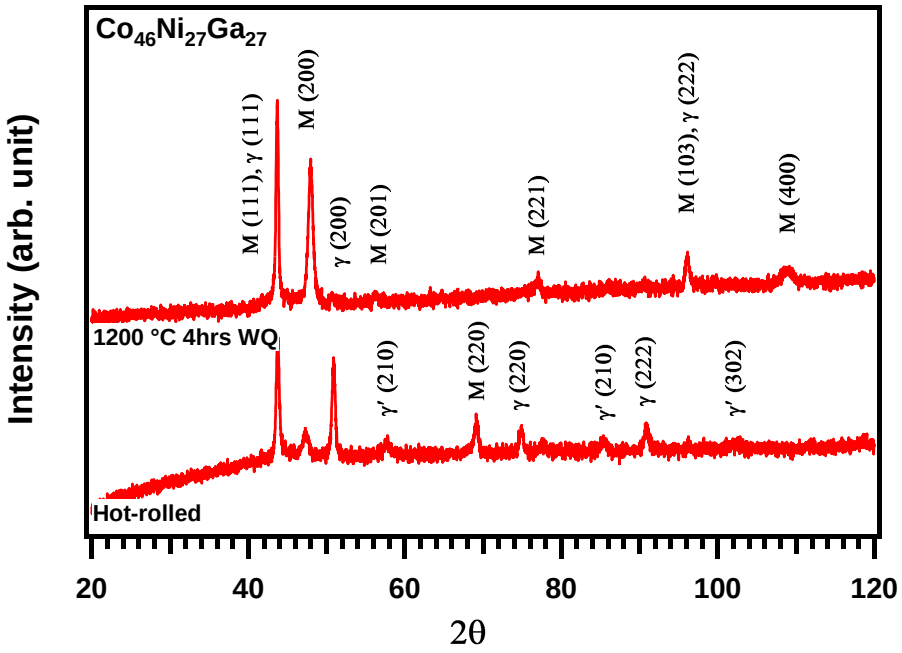


**Figure 3.3** X-ray diffraction pattern of bulk $Co_{46}Ni_{27}Ga_{27}$ samples after heat treated at 1200 °C for 4 hrs and hot rolling at 900 °C indicating the structures of the constitutive phases. M:$L1_0$ Martensite, γ: A1 structure (disordered fcc), γ`:$L1_2$ structure (ordered fcc).

However hot-rolled sample has three phase structure as shown in Figure 3.3. The lattice parameters of $L1_0$ martensite, γ and γ' phases are determined to be: 0.384 nm and c: 0.315 for martensite, a: 0.3585 nm for the fcc γ, and a: 0.359 for the fcc γ`. The c/a ratio of martensite phase is found to be 0.82.

Figure 3.4 displays the X-ray diffraction pattern of the two phase $Co_{46}Ni_{24}Ga_{30}$ and single phase $Co_{44}Ni_{26}Ga_{30}$ samples after heat treated at 1200°C for 4 hrs. The lattice parameter of the $L1_0$ martensite in the single phase $Co_{44}Ni_{26}Ga_{30}$ sample homogenized at 1200 °C is measured as a=0.381 nm and c: 0.324. Martensite lattice parameters were determined for $Co_{46}Ni_{24}Ga_{30}$ sample as a=0.3815 nm and c: 0.304 nm. The lattice parameter of γ is a: 3.567 nm for $Co_{46}Ni_{24}Ga_{30}$ sample.

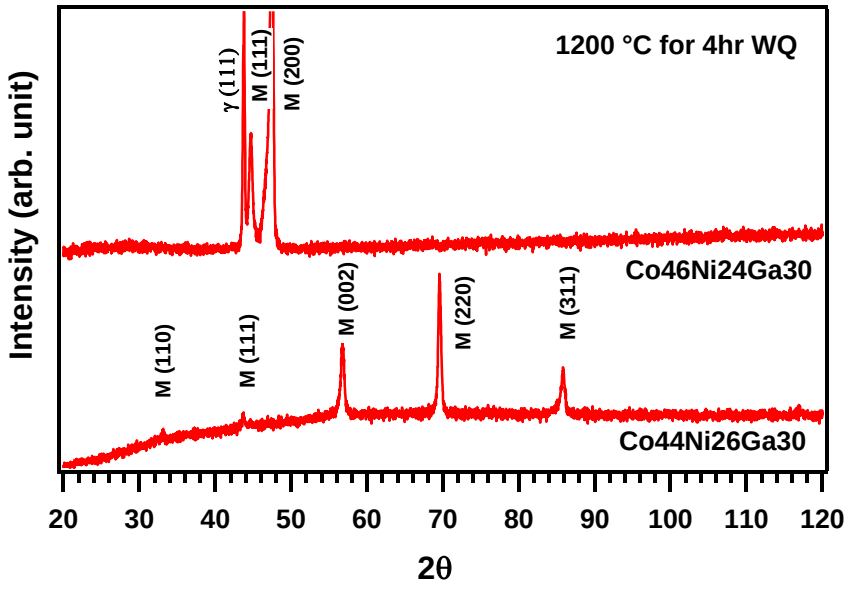


**Figure 3.4** X-ray diffraction pattern of bulk $Co_{46}Ni_{24}Ga_{30}$ and $Co_{46}Ni_{24}Ga_{30}$ samples after heat treated at 1200°C for 4 hrs indicating the structures of the constitutive phases .M:$L1_0$ Martensite, γ: A1 structure (disordered fcc).

### 3.3 DSC Results

One of the issues in HTSMAs is the transformation stability upon thermal and thermo-mechanical cycling due to diffusional mechanisms, at high temperatures such as creep, structural ordering, decomposition, and precipitation, precipitation, in addition to martensitic transformation. Present study is the first to investigate the transformation stability in CoNiGa HTSMAs. Firstly, CoNiGa alloys having $M_s$ of >150°C are presented. Table 3.2 shows transformation temperatures of the samples after heat treatment conditions presented in Table 3.1. The table also includes the quantative assessment of transformation temperature stability after successive thermal cycles (at least 5) within temperature range of 0 to 500 °C in the DSC. Thermal instability has been observed in some as-cast and heat treated $Co_{46}Ni_{27}Ga_{27}$ and $Co_{44}Ni_{26}Ga_{30}$ samples. When the transformation temperatures and transformation enthalpies change in each cycle notable, it is called unstable.

**Table 3.2** Transformation temperatures of $Co_{46}Ni_{27}Ga_{27}$ and $Co_{44}Ni_{26}Ga_{30}$ HTSMAs after few selected heat treatment conditions determined using DSC. $M_f$: Martensite finish, $M_s$: Martensite start, $A_s$: Austenite start, $A_f$: Austenite finish temperatures. $\Delta T$: $A_f$-$M_s$. When the transformation temperatures and transformation enthalpies change in each cycle notable it is called unstable.

| **Nominal Composition** | **Heat treatment** | **Transformation Temperatures (°C)** | | | | | **Thermal Cyclic Stability** |
|---|---|---|---|---|---|---|---|
| | | **$M_f$** | **$M_s$** | **$A_s$** | **$A_f$** | **$\Delta T$** | |
| $Co_{46}Ni_{27}Ga_{27}$ | 1200 °C 4hrs WQ | 294 | 318 | 461 | 494 | 176 | Unstable |
| $Co_{46}Ni_{27}Ga_{27}$ | Initial-HT | 214 | 243 | 392 | 434 | 191 | Unstable |
| $Co_{46}Ni_{27}Ga_{27}$ | Initial-HT<br>1150 °C 24 hrs WQ | 191 | 233 | 417 | 453 | 220 | Unstable |
| $Co_{46}Ni_{27}Ga_{27}$ | Initial-HT<br>1200 °C 24 hrs WQ | 200 | 247 | 442 | 472 | 225 | Unstable |
| $Co_{46}Ni_{27}Ga_{27}$ | Initial-HT<br>900 °C Hot rolled | 133 | 172 | 156 | 210 | 38 | Stable |
| $Co_{46}Ni_{27}Ga_{27}$ | Initial-HT<br>900 °C Hot rolled<br>1000 °C 1hr WQ | 200 | 231 | 350 | 420 | 187 | Stable |
| $Co_{46}Ni_{27}Ga_{27}$ | Initial-HT<br>900 °C Hot rolled<br>1200 °C 6 Days WQ | 264 | 281 | 444 | 469 | 188 | Unstable |
| $Co_{44}Ni_{26}Ga_{30}$ | 1200 °C 4 hr | 147 | 178 | 182 | 210 | 32 | Unstable |
| $Co_{44}Ni_{26}Ga_{30}$ | 1200 °C 4 hr<br>900 °C 24 hrs AC | 107 | 119 | 131 | 158 | 39 | Stable if temperature interval is 0 to 230°C /Unstable if it is 0 to 450°C |

Firstly, in this part, DSC results of the samples having $M_s$ higher than 150 °C are presented**.** Figures 3.5.a and 3.5.b picture the DSC responses of the $Co_{46}Ni_{27}Ga_{27}$ samples heat treated at 1200 °C for 4 hrs and initial-HT+1150 °C for 24 hrs followed by water quenching conditions, respectively. Thermal hysteresis is very high, about 176 °C and 212 °C in Figures 3.5.a and 3.5.b, respectively. In addition to the conventional transformation peaks, there is also an additional wide exothermic peak in the first

heating cycles shown with the arrows in the figure, before the first reverse martensitic transformation occurs. In addition, $M_s$ shifts to lower temperatures in subsequent cooling-heating cycles. The transformation enthalpies of forward and reverse martensitic transformations decrease with the number of thermal cycles. In the sample heat treated at 1200 °C, severe degradation of the transformation temperatures and heat occurs when the upper cycle temperature of the thermal cycles range is 50 °C above the $A_f$ which are shown in second and third cycles of the Figure 3.5.b.

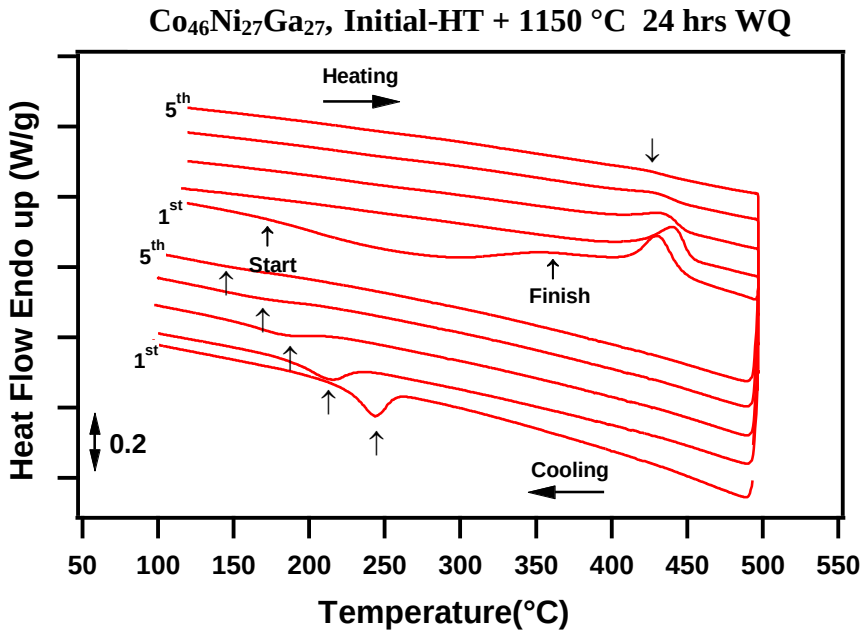


**(a)**

**Figure 3.5** DSC results of the $Co_{46}Ni_{27}Ga_{27}$ samples after the heat treatment at (a) 1150 °C for 24 hours followed by water quenching, after the initial-HT, and (b) 1200 °C for 4 hrs and water quenched.

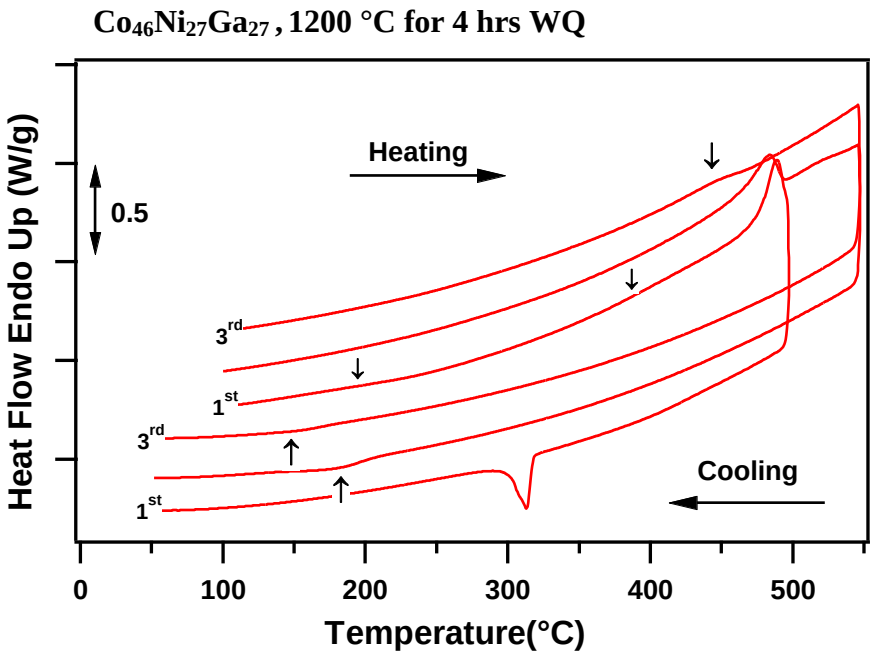


**(b)**

**Figure 3.5** Continued.

Unlike the unstable transformation temperatures presented in Figure 3.5, the hot rolled $Co_{46}Ni_{27}Ga_{27}$ samples showed relatively good thermal cyclic stability. Figures 3.6 pictures the DSC result of the hot rolled sample during successive thermal cycles. A stable transformation response is obvious when the sample is cycled between 50 and 500 °C. However, $M_s$ drops down to 151 °C from 172 °C when the upper cycle temperature is increased to 500 °C instead of 230 °C (Figures 3.6.b) and stay constant in the following cycles with the same upper cycle temperature. When the same sample is aged at room temperature for a few days, 10 days (Figures 3.6.b) and the DSC analysis is repeated the same scenario is observed. In other words, $M_s$ temperature is again 151 °C and 172 °C and stay constant in following cycles when upper cycle temperature is 230 °C and 500 °C, respectively. A similar wide exothermic peak as observed in Figure 3.5

is observed in the hot rolled sample (Figures 3.6b) when the upper cycle temperature is increased to 500 °C. The thermal hysteresis (Af-Ms) of hot-rolled sample is determined to 38 °C when the upper cycle temperature is 230 °C. This is the lowest stable transformation hysteresis level obtained the all samples having $M_s$ >150° investigated in this study.

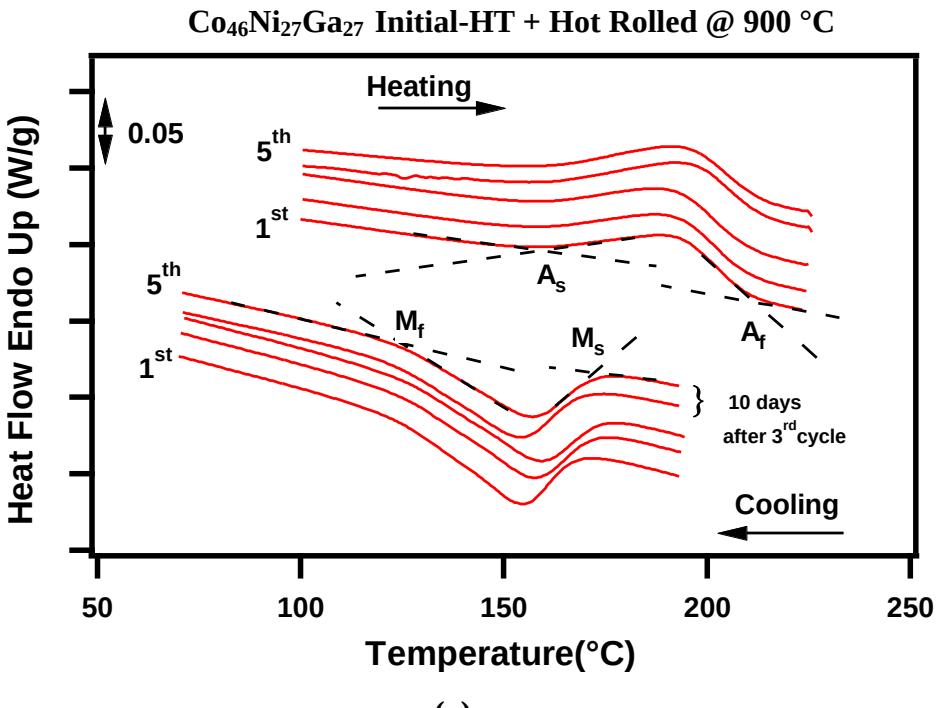


**(a)**

**Figure 3.6** DSC results of the hot rolled $Co_{46}Ni_{27}Ga_{27}$ sample (a) during three successive cycles and two more cycles after ten days aging at room temperature when the upper cycle temperature is 230 °C, and (b) when the upper cycle temperature is 500 °C.

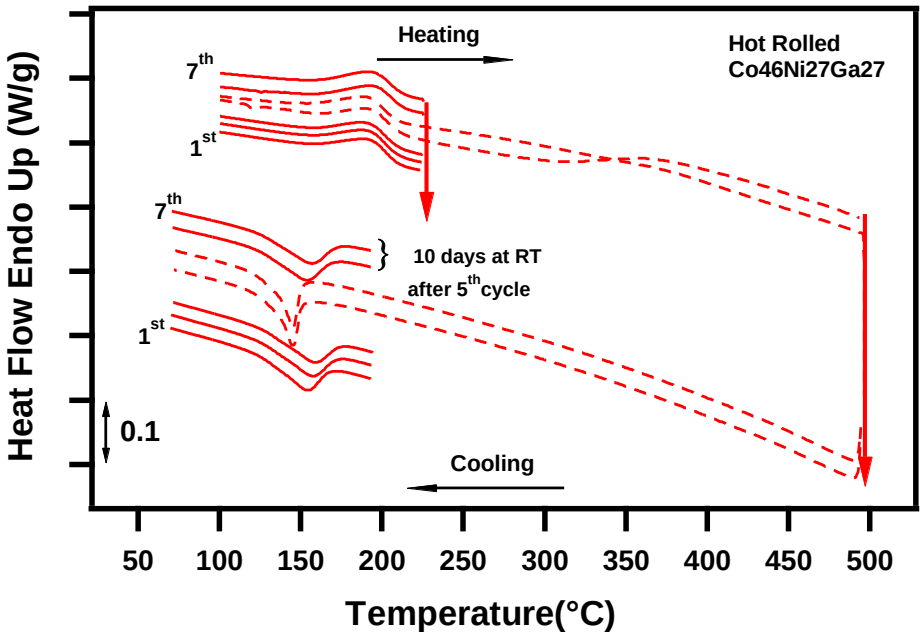


**(b)**

**Figure 3.6** Continued.

Figure 3.7 displays the DSC result of the hot rolled sample after annealing at 1000 °C for 1 hr followed by WQ. The heat treatment is performed to dissolve γ` phase in the matrix which is formed during slow cooling after hot rolling. Transformation temperatures of the annealed sample are very close to the transformation temperatures of the sample before hot rolling process (Table 3.2). The thermal hysteresis is again very high, about 187 °C and in the first heating cycle the wide exothermic peak appears as in Figure 3.5. However, unlike the instability in Figure 3.5 stable transformation temperatures are observed upon cycling in Figure 3.7. This indicates that γ` precipitates are not a necessary condition for the stable transformation response, point out that transformation stability is mainly controlled by the matrix composition.

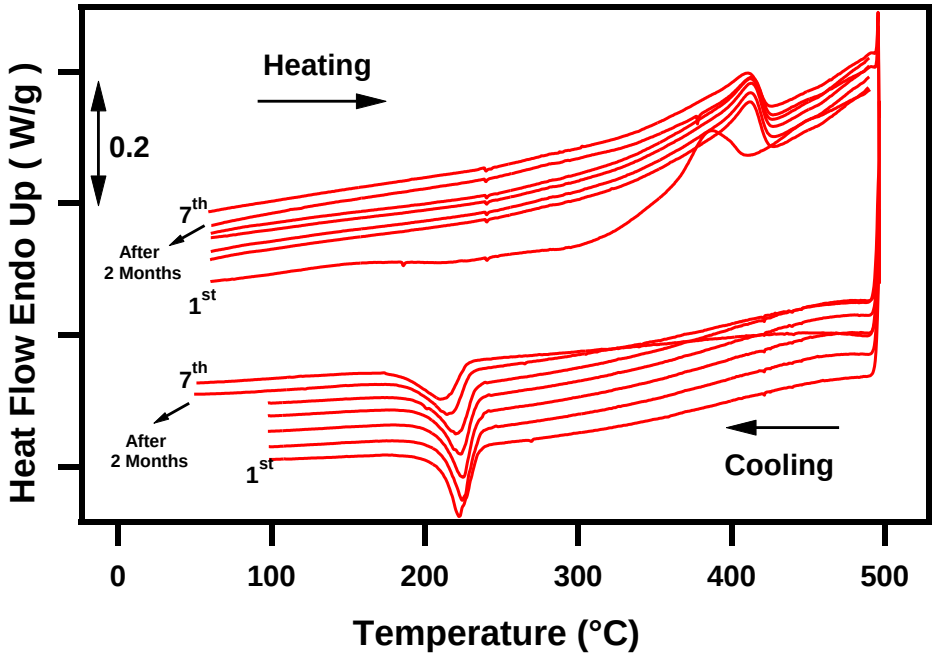


**Figure 3.7** DSC curves of the hot rolled $Co_{46}Ni_{27}Ga_{27}$ sample after annealed at 1000 °C during 5 successive cycles and two more cycles after 2 months.

The exothermic peak observed in Figure 3.5 and Figure 3.7 would be irreversible because it cannot be observed anymore when the DSC analysis is performed again for example after 2 months (Figure 3.7).

Figure 3.8 shows the DSC curve of $Co_{44}Ni_{26}Ga_{30}$ sample after heat treated at 1200 °C for 4 hrs. During five successive cycles, $M_s$ shifts to lower temperatures. In addition, the transformation enthalpies of forward and reverse martensitic transformations decrease with the number of thermal cycles. This observation resembles what is presented in Figure 3.5 for non-hot rolled $Co_{46}Ni_{27}Ga_{27}$ samples. Transformation instability and $M_s$ temperature drop with the number of cycles are observed in all

unstable $Co_{46}Ni_{27}Ga_{27}$ and $Co_{44}Ni_{26}Ga_{30}$ samples. However, in $Co_{44}Ni_{26}Ga_{30}$ alloy, the described behavior is slower than the $Co_{46}Ni_{27}Ga_{27}$ alloy cases (Fig 3.5 and Fig 3.8).

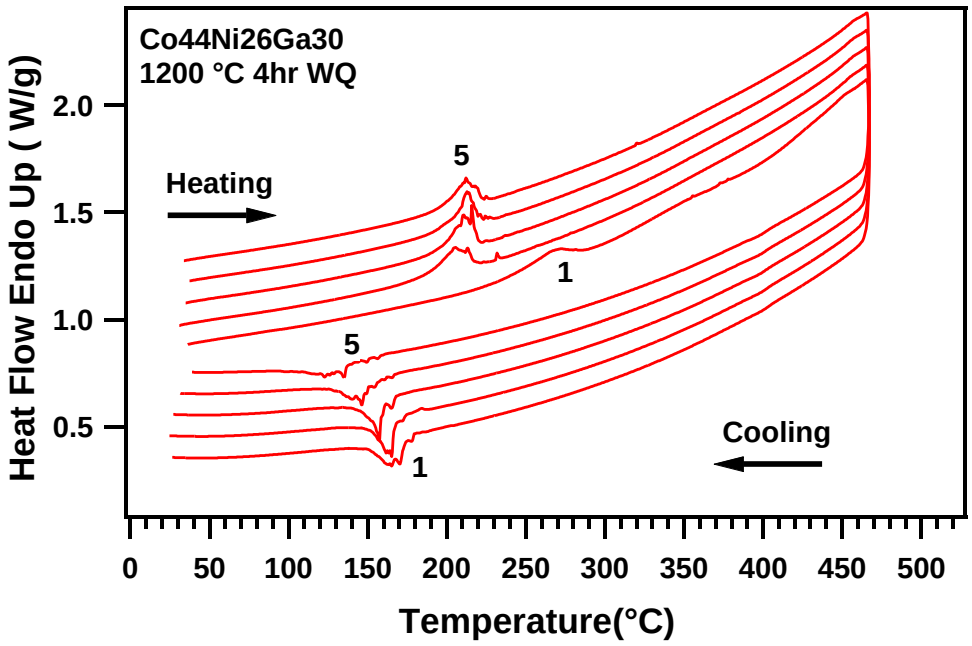


**Figure 3.8** DSC curves of the $Co_{44}Ni_{26}Ga_{30}$ sample after heat treated at 1200 °C for 4 hrs during 5 successive cycles.

When the same condition $Co_{44}Ni_{26}Ga_{30}$ sample in Figure 3.8 heat treated at 900 °C for 24 hrs and the DSC results are pictured in Figure 3.9, the sample showed stable transformation temperatures upon five successive DSC cycles when the upper cycle temperature is 230 °C. However, when the upper cycle temperature is 450 °C both the $M_s$ and $A_f$ shift to the higher temperatures upon cycling. There isn't notable change in transformation enthalpies with four thermal cycles. This is different than what is observed in some of the DSC figures showing instability above. In Figure 3.5 and Figure

3.8 above $M_s$ temperatures shift to lower temperatures upon thermal cycling and transformation enthalpies changes notable in each cycle.

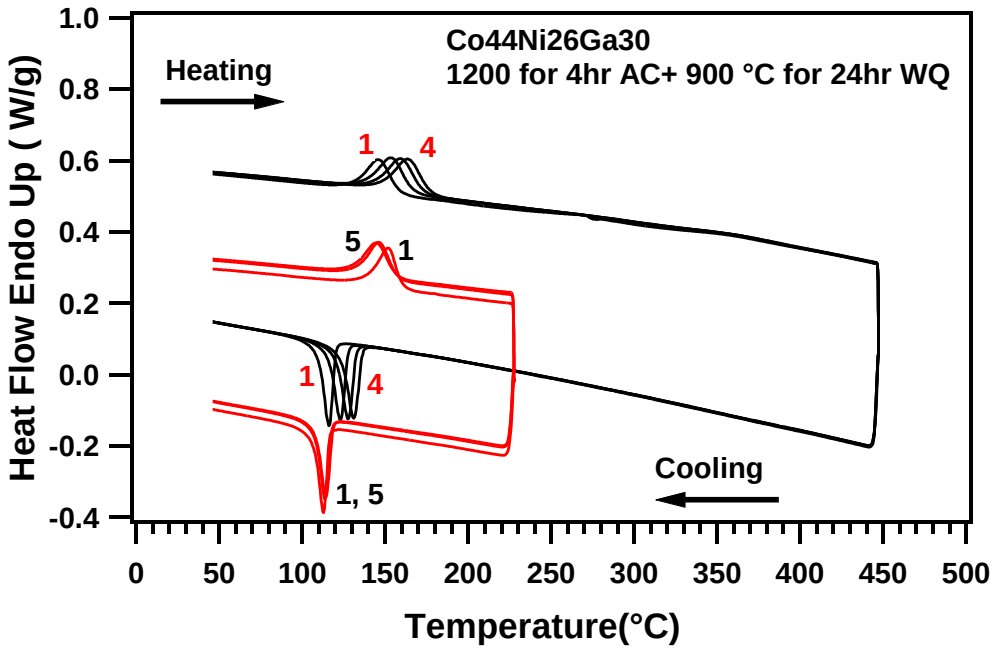


**Figure 3.9** DSC curves of the $Co_{44}Ni_{26}Ga_{30}$ sample after heat treated at 1200 °C for 4 hrs and 900°C for 24 hrs during 5 successive cycles.

After presenting the compositions that have $M_s$ of above 150 °C, DSC results of the some CoNiGa SMAs which have $M_s$ temperatures below 150 °C are introduced. Transformation temperatures and their behaviors upon thermal cycling of the heat treated at 1200 °C for 4 hrs $Co_{49}Ni_{22.5}Ga_{28.5}$ and $Co_{46}Ni_{24}Ga_{30}$ samples has been displayed in Figures 3.10.a and 3.10.b, respectively. $M_s$ temperatures are close to 100 °C and under stress it is expected to shift above 100 °C which can be considered a limit for HTSMAs.

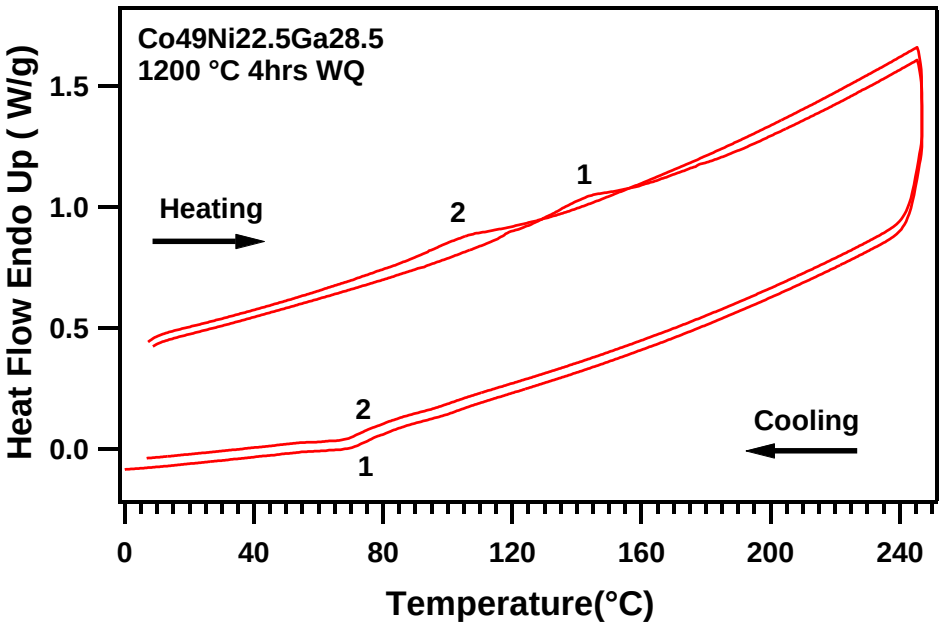


(a)

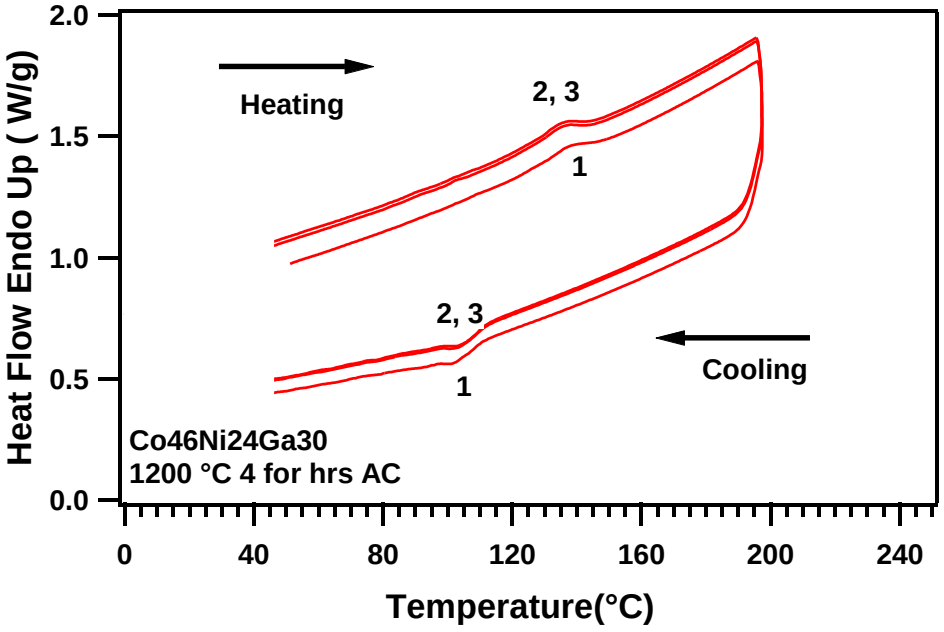


(b)

**Figure 3.10** DSC curves of the (a) $Co_{49}Ni_{22.5}Ga_{28.5}$ and (b) $Co_{46}Ni_{24}Ga_{30}$ samples after heat treated at 1200 °C for 4 hrs during 5 successive cycles.

### 3.4 TEM Results

In order to investigate the reason for instability of transformation temperatures and enthalpies during ongoing DSC cycles shown in Figure 3.5.b, homogenized at 1200 °C for 4 hrs and followed by water quenched $Co_{46}Ni_{27}Ga_{27}$ sample has been examined in in-*situ* TEM experiment. Sample was heated to austenite structure. Bright field TEM images at room temperature (RT) and just after the reverse martensitic transformation are shown in Figures 3.11.a and 3.11.d, respectively. Selected area electron diffraction patterns (EDPs) are taken from the areas indicated in Figures 3.11.a and 3.11.d and presented in the same figure. At RT, area 1 (Fig. 3.11.a) is martensite according to EDP in Figure 3.11.b. Area 2 is composed of twinned martensite, with $(1\bar{1}1)$ twinning plane according to the EDP shown in Figure 3.11.c. The structure of martensite is $L1_0$. During heating to reverse martensitic transformation occurs, new γ phase precipitates formed very fast in the matrix (Fig. 3.11.d). New γ phase precipitate, A1 structure, formed in area 1 (Fig. 3.11.e). However area 2 transforms to B2 according to the EDP shown in Figure 3.11.e. Therefore, it was found that thermal cyclic instability in DSC analysis is because of very fast γ phase precipitation formation in the matrix during heating which changed the matrix composition considerable and the volume fraction of transformable phases.

Since the hot rolled sample demonstrated the lowest transformation hysteresis and a stable transformation behavior, further investigated its transformation characteristics and the microstructural evolution using TEM with an in-situ heating stage. Bright field TEM images at room temperature (RT) and at 630 °C are shown in

Figures 3.12.a and 3.12.e, respectively. The sample has been heated in-situ to investigate the austenite structure, how martensite to austenite transformation occurs, and the thermal stability of both austenite and martensite. The sample stage was heated up to 630 °C where the martensite disappeared completely, and then the images were recorded. The reported temperatures may not be exactly the sample temperature since the stage temperature is measured and $A_f$ of the hot rolled sample is 210 °C from the DSC results. Selected EDPs are taken from the areas indicated in Figures 3.12.a and 3.12.e and presented in same figure. At RT, area 1 (Fig. 3.12.a) is composed of twinned martensite, with $(1\bar{1}1)$ twinning plane according to the EDP in Figure 3.12.b. Area 2 also has martensite structure with $(200)_M$ zone axis. The structure of martensite is $L1_0$. Area 3 is the γ phase. At 630 °C (Fig 3.12.e), the martensite in area 1 unexpectedly reverse transforms to B2 (β) and γ phases (Fig. 3.12.f) instead of only B2, with crystallographic relationships: $(1\bar{1}1)_M//(\bar{1}10)_{B2}//(11\bar{1})_\gamma$ and $[110]_M//[001]_{B2}//[011]_\gamma$ .It is not clear whether γ phase directly formed upon reverse transformation of martensite or martensite first transformed to B2 and then B2 transformed to γ heating up to 630 °C. It should be noted that $d_{(1\bar{1}1)_M}$ = 0.206 nm, which is very close to $d_{(11\bar{1})_\gamma}$ = 0.207 nm and $d_{(\bar{1}11)_{B2}}$ = 0.202 nm, so such transformation/precipitation (i. e M→β+ γ) may be possible. The pattern in Figure 3.12.f is slightly distorted especially at high angles, since it was recorded using large beam tilt as the orientation was out of the tilting range of the stage. The Area 2 transforms to β phase (Fig. 3.12.g) at 630°C. The area 3 is γ at RT and stay

mainly as γ phase at 630 °C. However, two precipitates appear in the γ phase near the β-γ interface, which is shown by the arrows in Figure 3.12.e.

Figure 3.12.i shows the microstructure of hot rolled sample at RT after heating up to 630 °C. In the EDPs from areas 1 and 2 (Fig. 3.12.j and 3.12.k ), martensite and weak reflections of γ′ are visible. The γ precipitates formed at 630 °C seem to undergo ordering to form γ′ at RT and B2 transforms to martensite. Area 3 (Fig 3.12.l ) is γ phase. Figure 3.12.m shows the appearance of fine γ′ precipitates in areas 1 and 2 after cooling down to RT. These fine precipitates are result of γ phase ordering which formed in the B2 matrix. However the massy γ′ precipitates indicated by arrows in Figure 3.12.i and shown in greater detail Figure 3.12.n nucleates and grows in the bulky γ region. This is reasonable because fine precipitates are because of the phase transformation (β→γ) and massy precipitates are results of ordering (γ→γ′), which occurs relatively faster than β→γ transformation. The size differences of γ′ precipitates in β and γ regions could be because of differences in β→γ transformation and γ→γ′ ordering reaction. In addition, the composition difference between β and γ phase should have also effect on the size of the γ` precipitates.

The EDP shown in Figure 3.12.o is obtained from the γ` precipitates by tilting from $[011]_{\gamma}$ to $[114]_{\gamma}$ for 33°. Interestingly, the strong intensity spots, as indicated by circles, are indexed as the γ phase, while extra reflections appear at the half spacing positions, indicating a double sized superlattice structure for the γ` phase. There are several types of fcc-based superlattice structures, such as $L1_0$, $L1_2$, and $D0_{22}$. The $D0_{22}$ is

derived from two $L1_2$ unit cells demonstrated in Figure 3.12.p. Here, the observed structure for the γ` phase is the supperlattice structure of 2×2×2 $L1_2$ unit cells. Energy Dispersive X-Ray Spectroscopy (EDS) analysis yielded the composition of $Co_{58.5}Ni_{20.4}Ga_{21.1}$ for the γ phase, and $Co_{53.2}Ni_{18.1}Ga_{28.7}$ for the γ` precipitates which is very close to $(CoNi)_3Ga$ form [43, 61]

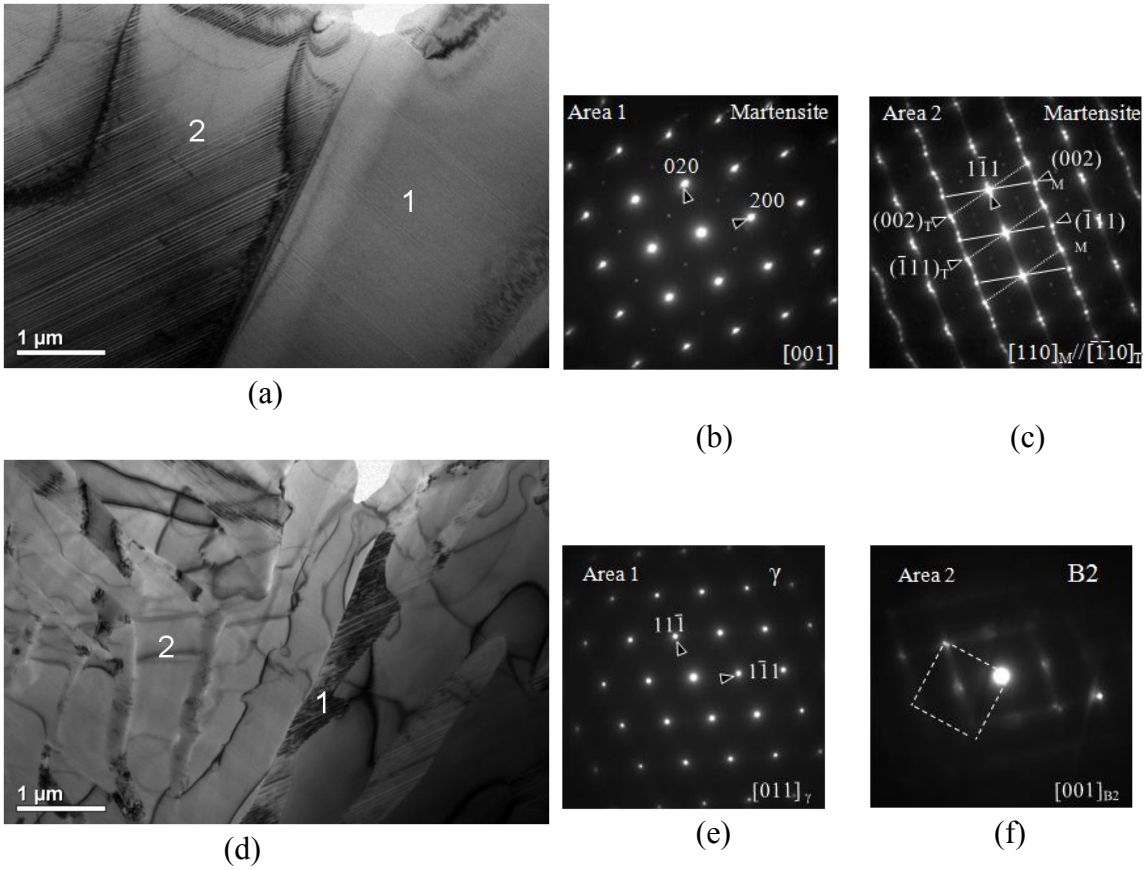


**Figure 3.11** (a) Bright field TEM image of the hot rolled $Co_{46}Ni_{27}Ga_{27}$ sample at room temperature. Selected area electron diffraction patterns (EDPs) of (b) area 1 and (c) area 2 shown in (a) indicating twinned structure of martensite. (d) Bright field TEM image at 670 °C. EDPs of (e) area 1 and (g) area 2 as shown in (d) which corresponds to same region of the foil in (a), presenting γ phase (e) and B2 (f) structure at the same time suggesting that the γ phase forms during in-*situ* TEM heating.

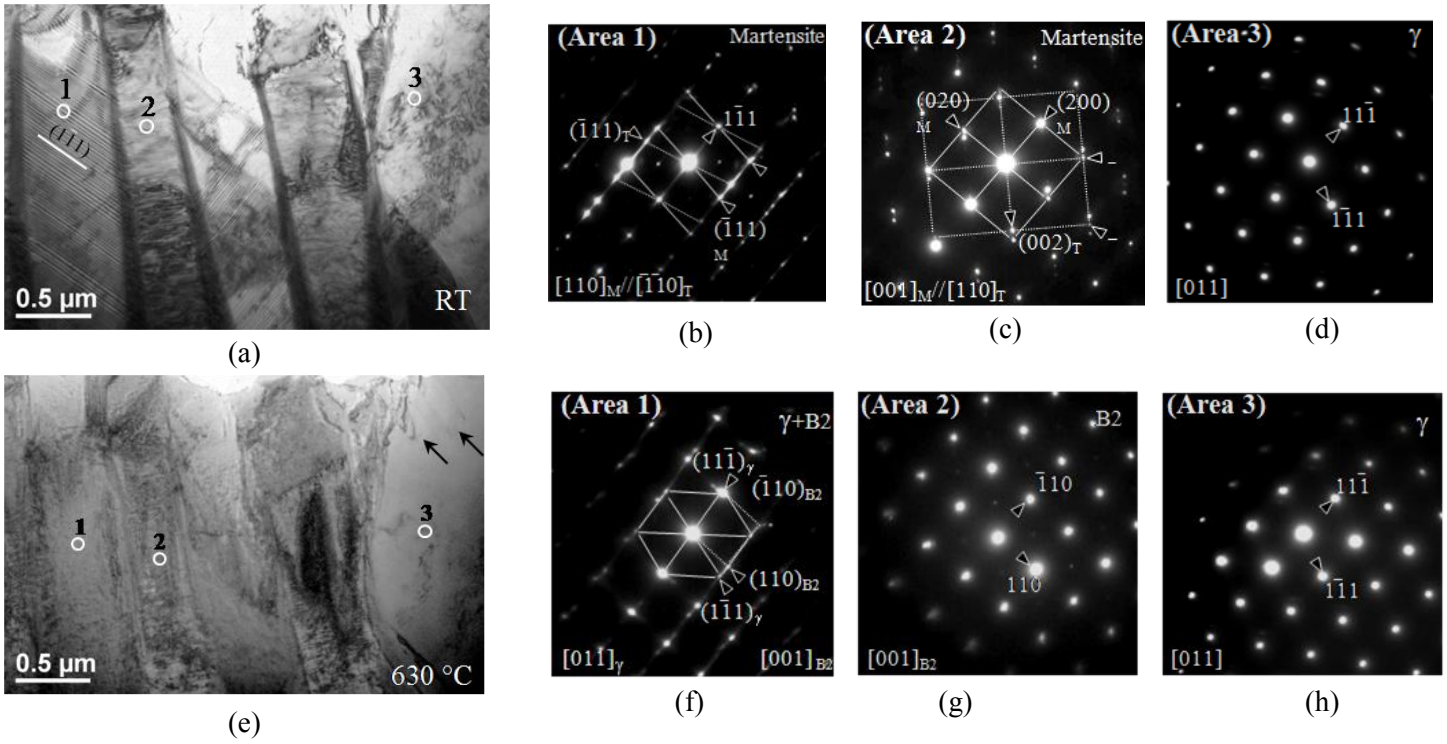


**Figure 3.12** (a) Bright field TEM image of the hot rolled $Co_{46}Ni_{27}Ga_{27}$ sample at room temperature. Selected area electron diffraction patterns (EDPs) of (b) area 1, (c) area 2 and (d) area 3 as shown in (a). (e) Bright field TEM image at 630 °C. EDPs of (f) area 1, (g) area 2 and (h) area 3 as shown in (e) which corresponds to same region of the toil in (a). (i) Bright field TEM image after cooling down to room temperature, EDPs from (j) area 1, (k) area 2, (l) area 3 and as shown in (i). (m) Enlarged bright field image of area 1 and area 2. (n) Dark field image of the precipitates formed in area 3, and (o) EDP of γ` formed in γ phase region in (n). (p) Unit cell demonstration of $L1_2$ , $D0_{22}$ supperlattice structure and supper lattice structure of γ` phase in the present work. M: Martensite, T: Twin, B2: Austenite, γ: Gamma phase (A1), γ`: Gamma prime phase ($L1_2$).

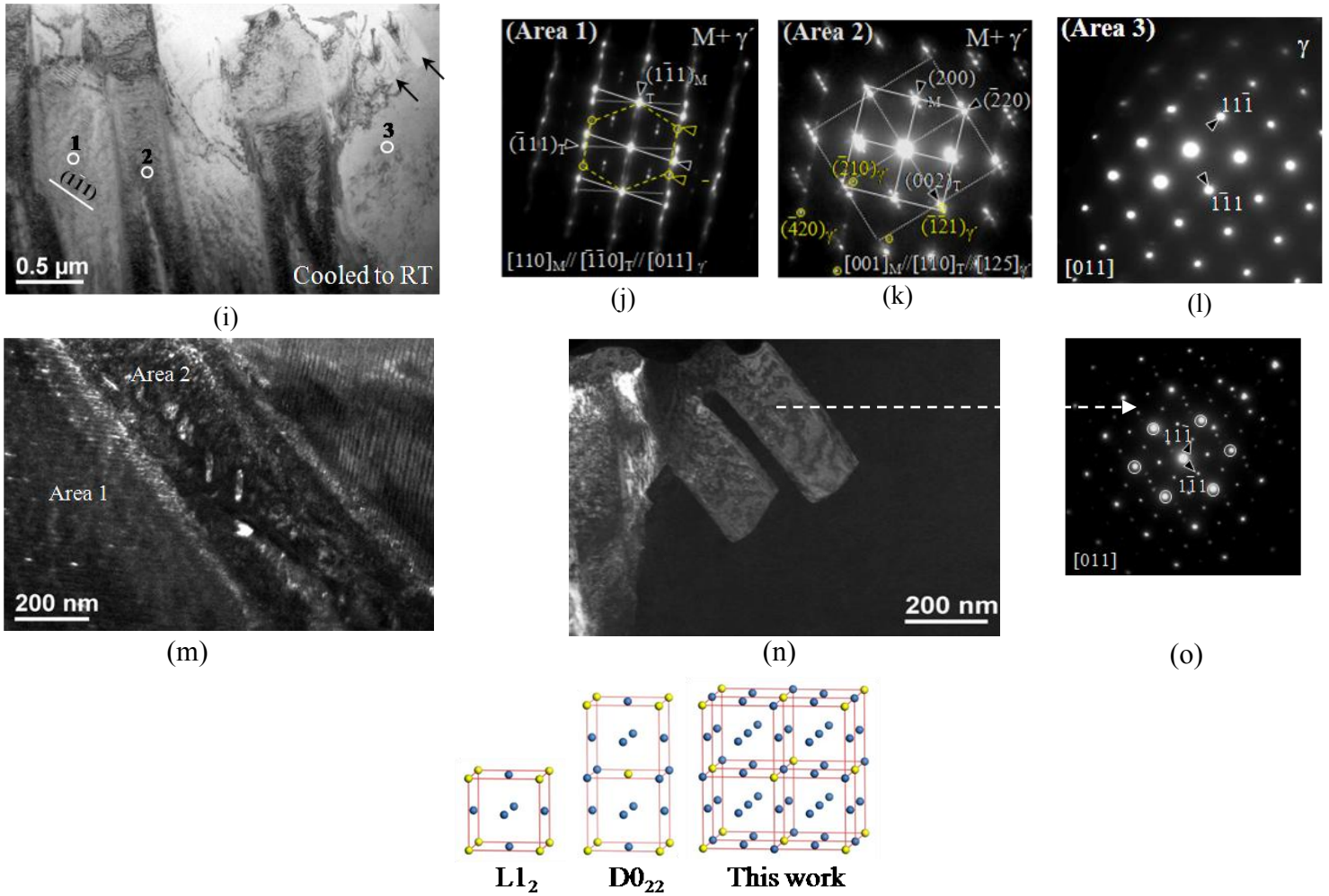


**Figure 3.12** Continued.

### 3.5 Thermo-Mechanical Processing of $Co_{46}Ni_{27}Ga_{27}$ and $Co_{44}Ni_{26}Ga_{30}$ HTSMAs

Figure 3.13 presents microstructures of $Co_{46}Ni_{27}Ga_{27}$ and $Co_{44}Ni_{26}Ga_{30}$ alloys before hot rolling process. Figure 3.13.a shows the optical micrograph of initial-HT $Co_{46}Ni_{27}Ga_{27}$ alloy with 28% γ phase volume fraction before hot rolling process at 900 °C. Figure 3.13.b displays the optical micrograph of $Co_{46}Ni_{27}Ga_{27}$ alloy heat treated at 1200 °C for 4 hrs followed by WQ and annealed at 1000 °C for 24 hrs followed by WQ which has 14% γ phase volume fraction. $Co_{44}Ni_{26}Ga_{30}$ alloy has 6 % γ phase volume fraction after homogenization at 1200 °C for 4 hrs and annealed at 900 °C for 24 hrs (Fig. 3.13.c). Table 3.13 presents the list of these CoNiGa alloys with their heat treatment conditions, rolling temperature, γ phase volume fraction, conditions and specifications, initial thickness of the sample, total thickness reduction achieved and thickness reduction in each passes. Initial-HT $Co_{46}Ni_{27}Ga_{27}$ sample having 28% γ phase volume fraction was hot rolled successfully at 900 °C with thickness reduction of 40%. The $Co_{46}Ni_{27}Ga_{27}$ sample, homogenized at 1200 °C for 4 hrs and annealed at 1000 °C for 24 hrs, with 14% γ phase volume fraction has also been hot rolled to 40% thickness reduction successfully, but at a lower temperature, 800 °C. It was not possible to hot roll the same sample with 14% γ phase volume fraction at 700 °C due to the grain boundary cracking after the first three rolling passes (Fig 3.14.a). The $Co_{44}Ni_{26}Ga_{30}$ sample heat treated at 1200 °C for 4 hrs WQ + 900 °C for 24 hrs AC has only 6% γ phase volume fraction and was hot rolled at 900 °C unsuccessfully (Fig 3.14.b). It was concluded that more than 10% γ phase volume fraction is necessary for successful thermo-mechanical processing of CoNiGa alloys which suffer from intergranular fracture (Fig 3.14).

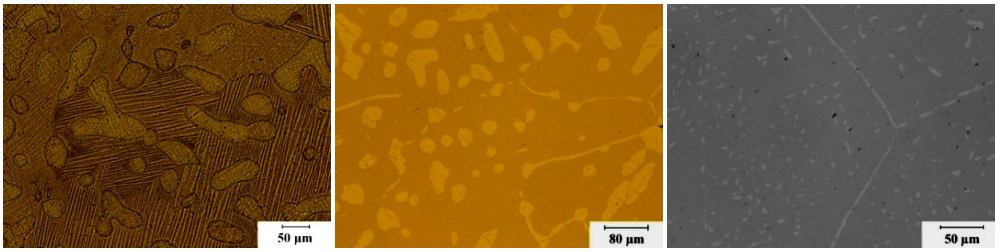


(a) (b) (c)

**Figure 3.13** Optical micrographs of $Co_{46}Ni_{27}Ga_{27}$ samples after (a) 1150°C for 8 hr + 1100°C for 24 hrs followed by air cooling, (b) 1200°C for 4 hrs WQ + 1000°C for 24 hrs WQ, and (c) $Co_{44}Ni_{26}Ga_{30}$ after 1200°C for 4 hrs WQ + 900°C for 24 hrs AC and before hot rolling processes.

**Table 3.3** List of thermo-mechanical processes conducted on $Co_{46}Ni_{27}Ga_{27}$ and $Co_{44}Ni_{26}Ga_{30}$ alloys.

| | | **Heat treatment** | **Rolling Temp** | **Gamma Volume fraction** | **Conditions, Specifications** | **Initial thickness** | **Reduction %** | **Passes** |
|---|---|---|---|---|---|---|---|---|
| **a** | **Co46Ni27Ga27** | 1150 °C 8 hr+ 1100 °C 24 hr AC | 900 °C | 28 | In steel can. Successfully processed | 6.7mm | 40 | 10%,10%,5%..... |
| **b** | **Co46Ni27Ga27** | 1200 °C 4hrs WQ +1000 °C 24 hrs WQ | 800 °C | 14 (Not homogeneously distributed) | Non-canned sample. Successfully processed | 2 mm | 41 | 16%,10%,10%,15% |
| **b** | **Co46Ni27Ga27** | 1200 °C 4hrs WQ +1000 °C 24 hrs WQ | 700 °C | 14 | Non-canned sample. It seriously cracked along grain boundaries. | 7 mm | 24.5 | 6%,10%, 10% |
| **c** | **Co44Ni26Ga30** | 1200 °C 4hrs AC+ 900 °C 24 hrs AC | 900 °C | 6 | Non-canned sample. It cracked severely along grain boundaries. after first two passes | 2.5 mm | 15% | 5%,10% |

(a) (b)

**Figure 3.14** Pictures of the heavily cracked samples after hot rolling process. (a) $Co_{46}Ni_{27}Ga_{27}$ sample heat treated at 1200°C for 4 hrs WQ + 1000°C for 24 hrs WQ, (b) $Co_{44}Ni_{26}Ga_{30}$ sample heat treated at 1200°C for 4 hrs WQ + 900°C for 24 hrs AC. Pictures show clearly how samples cracked along grain boundaries.

### 3.6 Low Temperature Aging of $Co_{44}Ni_{26}Ga_{30}$ HTSMA

The influence of low temperature annealing on $Co_{44}Ni_{26}Ga_{30}$ HTSMA has been studied, which can cause γ' phase precipitation. The $Co_{44}Ni_{26}Ga_{30}$ samples homogenized at 1200 °C for 4 hrs and followed by water quenching were aged at different temperatures (250 °C – 400 °C) to investigate the change in transformation temperatures. Aging at 300 °C gives the most promising transformation temperatures in terms of the low thermal hysteresis; therefore, the samples were aged at 300 °C for different durations. Table 3.15 presents the list of heat treatments, transformation temperatures, and upper cycle temperature for the DSC analysis.

Annealing at 250 °C does not change transformation temperatures notably, however, aging at 300 °C for 1 hr decreases them, and when the sample is aged more at 300 °C, for example, for more than 4 hrs, the thermal hysteresis increases, even though $M_s$ does not change much. Aging at 350 °C for 1 hr also decreased the transformation temperatures. When the sample is aged at 400 °C, no transformation was observed in the DSC analysis down to -60°C. Very low thermal hysteresis of 15 °C was obtained after annealing at 300 °C for 1 hour as shown in Figure 3.15.

**Table 3.4** List of heat treatments, transformation temperatures in three cycles, and upper cycle temperature of the DSC analysis for the $Co_{44}Ni_{26}Ga_{30}$ samples.

| | **$M_s$ (°C) Cycle** | | | **Comment** | **$A_f$ (°C) Cycle** | | | **Upper Cycle Temperature (%)** |
|---|---|---|---|---|---|---|---|---|
| **Heat Treatment** | **1** | **2** | **3** | | **1** | **2** | **3** | |
| 1200°C 4hrs WQ | 170 | 176 | 169 | Decreasing enthalpy | 373 | 210 | 235 | 450 |
| + 250 C 1 hr WQ | 170 | 170 | 170 | Not remarkable change in enthalpy | 388 | 218 | 233 | 450 |
| + 300 C 1 hr AC | 108 | 108 | *ND* | Not remarkable change in enthalpy | 125 | 123 | *ND* | 220 |
| + 300 C 1 hr AC + 300 C 4hrs AC | 109 | 106 | *ND* | Not remarkable change in enthalpy | 181 | 181 | *ND* | 220 |
| + 300 C 24 hrs AC | 188 | 194 | 182 | Decreasing enthalpy | 431 | 230 | 404 | 450 |
| + 350 C 1 hr WQ | 134 | 102 | 65 | Decreasing enthalpy | 229 | 210 | 214 | 450 |
| + 400 C 1 hr WQ | No peak | No peak | No peak | Decreasing enthalpy | No peak | No peak | No peak | 450 |

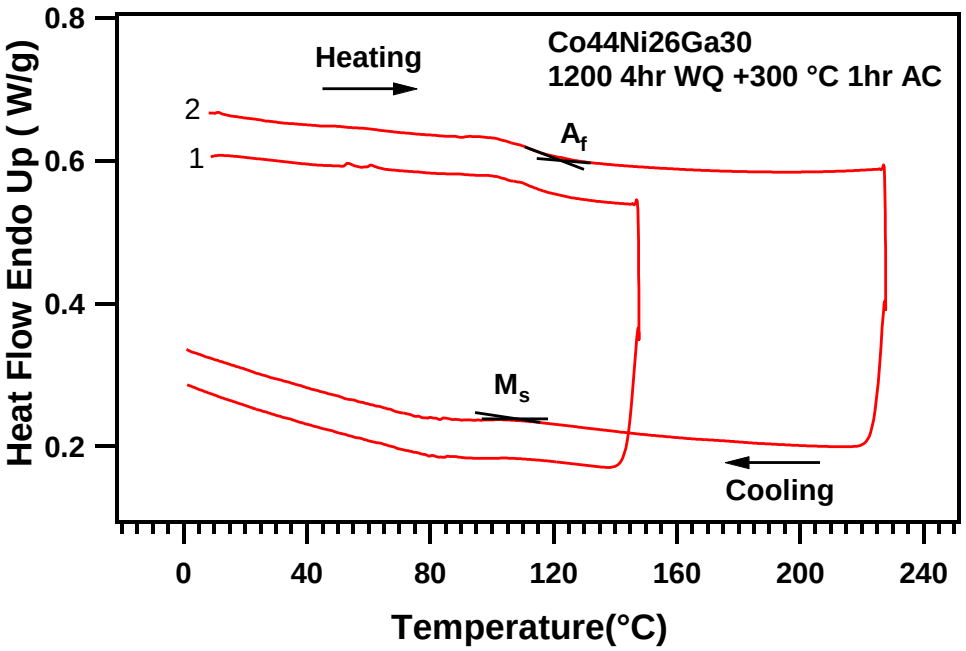


**Figure 3.15** DSC response of the $Co_{44}Ni_{26}Ga_{30}$ samples after homogenization at 1200°C for 4 hrs and heat treated at 300°C for 1 hr followed by air cooling.

### 3.7 Mechanical and Shape Memory Test Results

Both tension and compression yield tests are conducted for hot rolled $Co_{46}Ni_{27}Ga_{27}$ samples to reflect the plasticity of the alloy. The sample exhibited very high tension-compression asymmetry which is mostly due to intergranular fracture mechanism. Only 2% yield strain is recorded for hot rolled $Co_{46}Ni_{27}Ga_{27}$ sample after tension yield test where sample is failed along grain boundaries. Figure 3.16 demonstrates stress strain responses of the hot rolled, hot rolled and annealed at 1000°C 1 hr samples. After annealing at 1000°C for 1 hr, the γ` phase precipitates dissolved, however volume fraction of the γ phase did not change. From the Figure 3.16 γ` effect

on modulus and yield stress is obvious, on the other hand maximum strain value is smaller when γ` precipitates present.

Figure 3.17 pictures the microstructure of the hot rolled and 1000°C for 1 hr and water quenched $Co_{46}Ni_{27}Ga_{27}$ sample after yield test as shown in Figure 3.16. It is obvious from the figure that sample failed along grain boundaries. In addition, crack propagation is prevented by γ phase particles which is further confirmation that γ phase has significant effect on ductility of CoNiGa SMAs. In addition, annealing twins have been observed in γ phase regions, which are due to heat treatment of heavily deformed sample at 1000 °C.

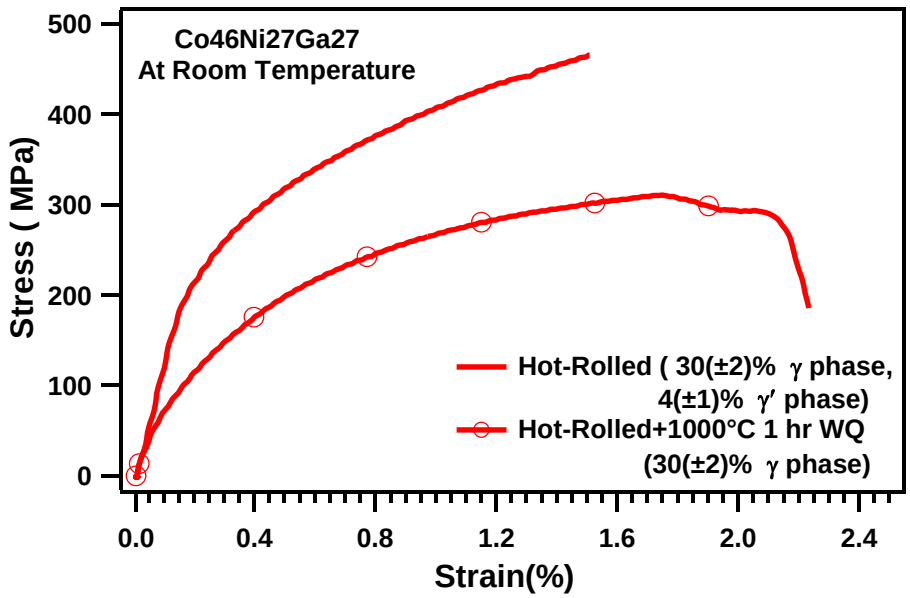


**Figure 3.16** Tension stress strain response of the hot rolled and hot rolled+1000 °C for 1 hr and water quenched $Co_{46}Ni_{27}Ga_{27}$ samples along rolling direction at room temperature indicating γ` phase effect on yield stress level.

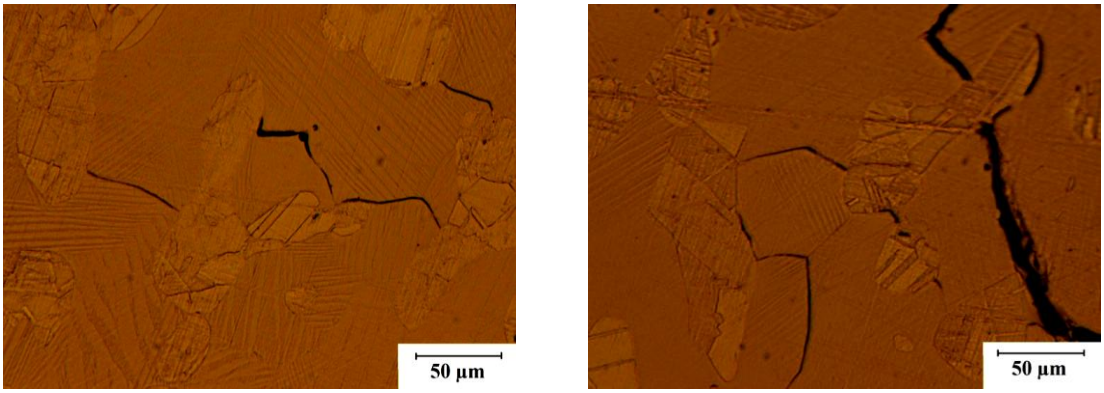


**Figure 3.17** Optical micrograph of the hot rolled and 1000 °C for 1 hr followed by water quenched $Co_{46}Ni_{27}Ga_{27}$ samples after yield test indicating intergranular fracture clearly. In addition cracks stop when they meet the γ phase particles.

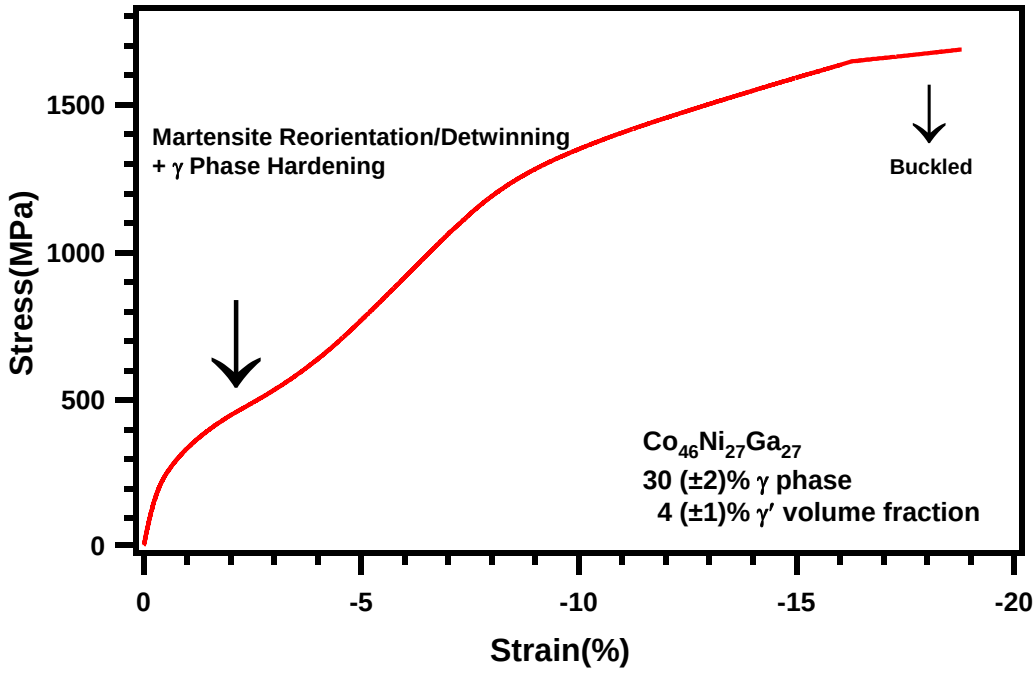


**Figure 3.18** Compression stress strain response of the hot rolled $Co_{46}Ni_{27}Ga_{27}$ samples along the rolling direction at room temperature indicating distinct martensite reorientation/detwinning plateau.

Figure 3.18 presents the compressive stress-strain curve of the hot rolled $Co_{46}Ni_{27}Ga_{27}$ sample at room temperature. The sample buckled above 16% compressive strain as indicated in the figure. The stress plateau indicated by the arrow in the first stage of the stress strain curve corresponds to martensite reorientation/detwinning and probably γ phase hardening processes. The hardness value of the γ phase increased from 266 HV to 305 HV and the matrix hardness stepped up from 314 HV to 392 HV after the test.

Figure 3.19 demonstrates strain vs. temperature response of the hot rolled $Co_{46}Ni_{27}Ga_{27}$ samples along the transverse direction under various constant tension stress levels. The shape change during the cooling upon martensitic transformation demonstrates the transformation strain level. The transformation strain levels are found to be larger along the transverse direction which is should be due to the crystallographic texture effect. The maximum transformation strain obtained was 0.25 % under 250 MPa with almost no recovery.

Figure 3.20 displays compression stress-strain response of the hot rolled $Co_{46}Ni_{27}Ga_{27}$ samples along the rolling direction. Sample is loaded up to 2 % strain in martensite form at room temperature then unloaded which caused about 1.4% residual strain. When the sample is heated above $A_f$, 0.25% strain recovery was pictured due to the reverse martensitic transformation.

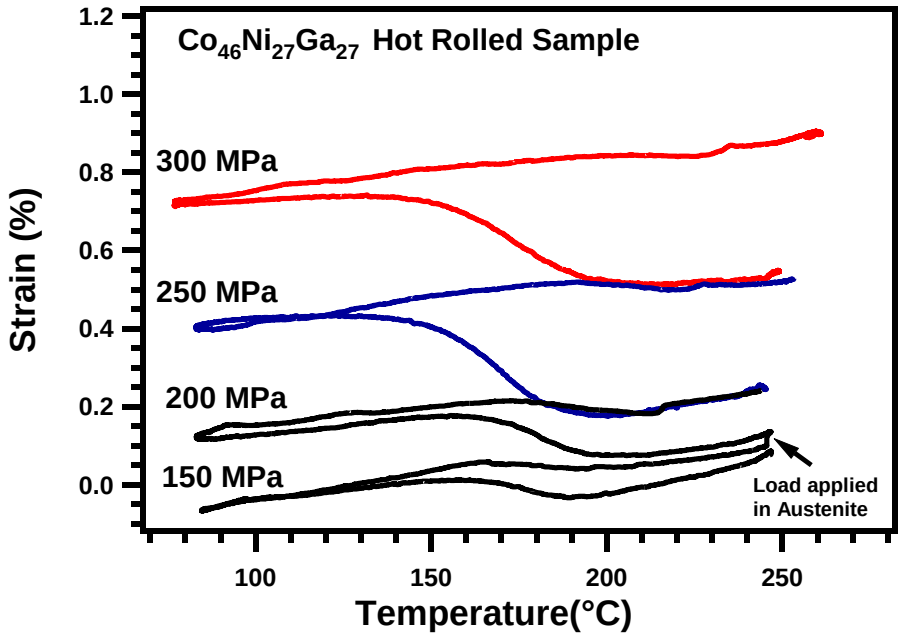


**Figure 3.19** Strain vs. temperature response of the hot rolled $Co_{46}Ni_{27}Ga_{27}$ samples along the transverse direction under various tensile bias stress levels.

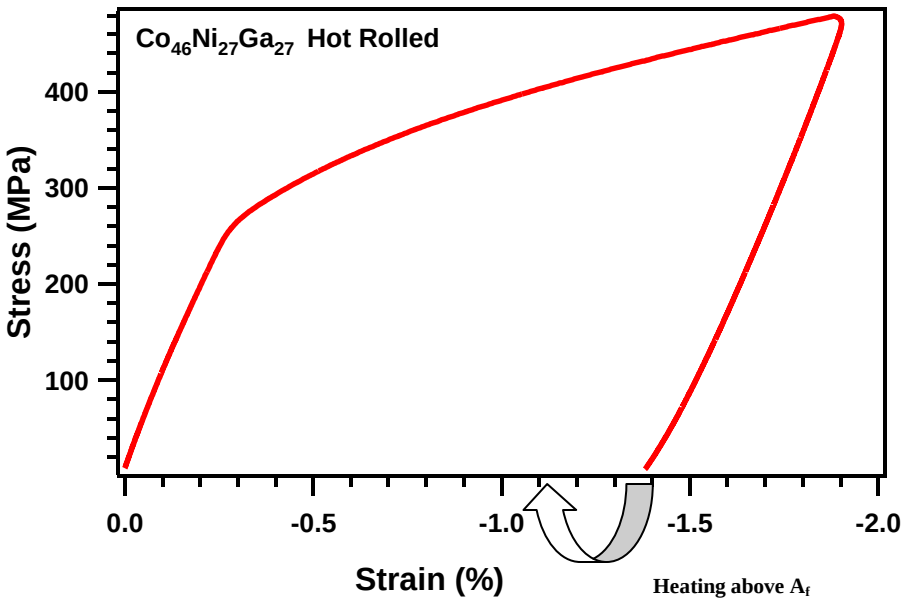


**Figure 3.20** Compression stress strain response of the hot rolled $Co_{46}Ni_{27}Ga_{27}$ sample along the rolling direction. Sample is deformed about 2 % strain in martensite at room temperature, after that sample is heated above $A_f$ which caused 0.25 % strain recovery.

Figure 3.21 pictures compression stress-strain response of the $Co_{46}Ni_{27}Ga_{27}$ sample. The sample is loaded up to 2.2 % strain in martensite , at room temperature, then unloaded which caused about 1.5% residual strain. When the sample is heated above $A_f$ , 1.24 % strain recovery was recorded upon a reverse martensitic transformation. The recovered strain is 78% of the residual strain after unloading, which is promising.

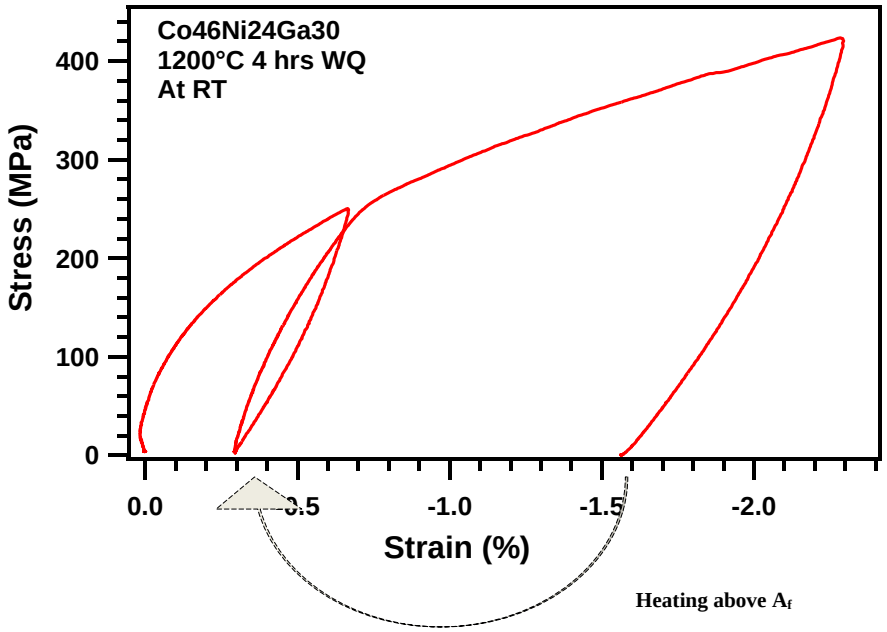


**Figure 3.21** Compression stress strain response of the $Co_{46}Ni_{24}Ga_{30}$ sample. Sample is deformed about 2 % strain in martensite, at room temperature, after that sample is heated above $A_f$ that caused 1.24% strain recovery. The recovered strain is 78% of the residual strain.

### 3.8 Single Crystal $Co_{49}Ni_{22.5}Ga_{28.5}$ HTSMAs

Figures 3.22.a and 3.22.b present the optical micrograph and DSC response of single crystalline $Co_{49}Ni_{22.5}Ga_{28.5}$ alloy, respectively. The single crystals were grown in a He environment using a Bridgman furnace. $Co_{49}Ni_{22.5}Ga_{28.5}$ HTSMA is selected to grow

single crystalline form because of its promising transformation temperatures. Characterization of the $Co_{49}Ni_{22.5}Ga_{28.5}$ SMAs is selected in single crystalline form to eliminate negative effect of polycrystalline on ductility and SME. As-grown sample showed two phase microstructure ($\beta+\gamma$) having $M_s$ of 72 °C with 28 °C thermal hysteresis. $\gamma$ phase volume fraction is determined as 16% in as-grown sample. The transformation temperature is expected to increase above 100 °C during isobaric thermal cycling experiments even when low stresses are applied according to previously studied $Co_{49}Ni_{21}Ga_{30}$ single crystalline alloy [35]. Isobaric thermal cycling experiments will be conducted for the single crystal $Co_{49}Ni_{22.5}Ga_{28.5}$ alloy.

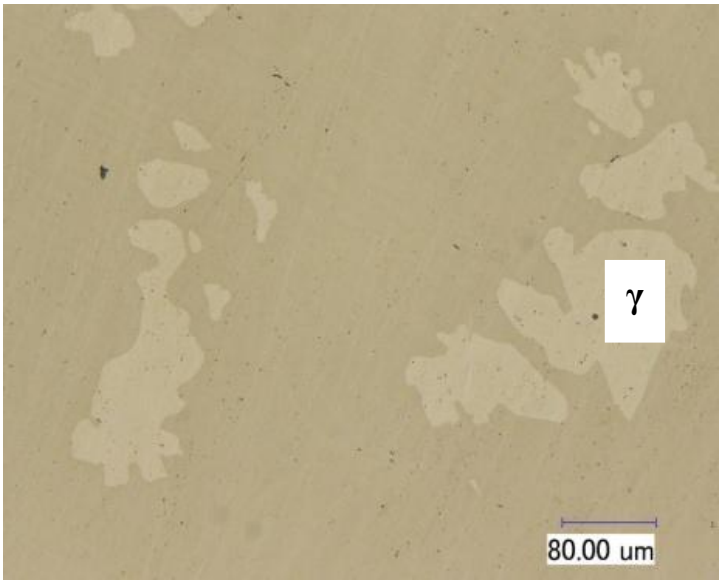


(a)

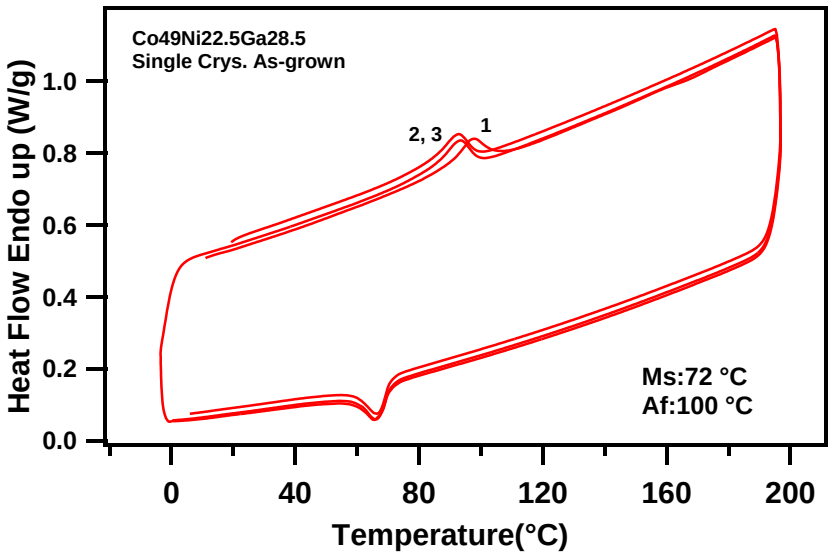


(b)

**Figure 3.22** (a) Optical micrograph and (b) DSC response of the single crystalline $Co_{49}Ni_{22.5}Ga_{28.5}$ at.% alloy.

# CHAPTER IV

# DISCUSSION OF EXPERIMENTAL RESULTS

## 4.1 Martensitic Transformation Characteristics of $Co_{46}Ni_{27}Ga_{27}$

In previous section the transformation temperatures evolution of some $Co_{46}Ni_{27}Ga_{27}$ samples upon DSC cycling have been presented. There are main and important observations; thermal hysteresis is very high in some samples (Fig. 3.5 and Fig. 3.7), thermal cyclic instability upon DSC cycling which is very sensitive to upper cycle temperature (Fig. 3.5.b), a wide exothermic peak in the first heating cycle before (Fig. 3.5 and Fig. 3.7) and after (Fig. 3.6.b) reverse martensitic transformation occurs. Hot rolled $Co_{46}Ni_{27}Ga_{27}$ samples displayed relatively good thermal cyclic stability with relatively low thermal hysteresis and the hot rolled sample $M_s$ temperature is very sensitive to the DSC upper cycle temperature (Fig. 3.6.b). In addition, $M_s$ temperature drops down by about 20°C when upper cycle temperature is 500 °C instead of 230 °C which is just above the $A_f$ temperature (Fig. 3.6.b). The $M_s$ decrease is reversible which means $M_s$ recovers temperature drop when it is aged at room temperature (Fig. 3.6.b). In this part, the reasons of the described observations above will be discussed with the new experiments presented below.

The transformation enthalpies decrease with number of cycles as presented in Figure 3.5 is because of the volume fraction of the transforming matrix decreases as a result of the very fast γ precipitations as shown in the TEM analysis (Fig. 3.11). In addition, $M_s$ temperature decreases during each cycle and after couple of cycle $M_s$ temperature cannot be distinguished because of the disappearing of transformation

enthalpies. When there is γ formation, $M_s$ temperature decrease is high and continuous upon cycling with the notable decreasing of the transformation enthalpies (Fig. 3.5 and Fig. 3.11). However, when γ` precipitates occurs $M_s$ temperature change is small and there is not notable change in the transformation enthalpies (Fig. 3.6.b and Fig. 3.12). To summarize, the instability and the transformation enthalpy decrease in the successive cycles shown in Figure 3.5 is as a result of the decomposition of the matrix and the change in the martensite volume fraction [60].

### 4.1.1 Effect of Aging in Different Phases

Thermal cyclic instability has been observed during subsequent cooling-heating cycles in the $Co_{46}Ni_{27}Ga_{27}$ sample after initial-HT and heat treatment at 1150 °C for 24 hrs WQ, as shown in Figure 3.5.b. In addition, thermal hysteresis is very high. A similar behavior is also observed in the $Co_{46}Ni_{27}Ga_{27}$ sample homogenized at 1200 °C for 4 hrs. In-situ TEM experiments as shown in Figure 3.11 indicate that γ phase precipitates causes thermal instability in subsequent heating-cooling cycles when the upper cycle temperature is 50°C above $A_f$ in the $Co_{46}Ni_{27}Ga_{27}$ sample heat treated at 1200 °C for 4 hrs.

Figure 4.1 displays in-*situ* DSC analysis of the $Co_{46}Ni_{27}Ga_{27}$ sample after initial-HT and heat treatment at 1150 °C for 24 hrs WQ, showing transformation temperatures behavior when the sample is aged in the martensite or austenite at 350 °C. Since the thermal hysteresis is very high and there is a wide temperature range where the martensite or austenite can exist, it is possible to age sample both in austenite and martensite at high temperatures. When sample is aged in martensite for 30 minutes there

is not any notable change in transformation temperatures. Aging in the austenite for 30 minutes causes about 20 °C decrease in $M_s$. When the sample is aged in the martensite again but for 3 hrs, $A_f$ temperature increased by 20 °C without any change in $M_s$. This can be attributed to the stabilization of the martensite due to symmetry conforming short range ordering which shifts the reverse transformation to higher temperatures. When the sample is aged again in the austenite but for 3 hrs, $M_s$ decreased about 40 °C. In all cases the transformation enthalpies are very close for first heating-cooling cycle no matter if aging is in austenite or martensite. What we can conclude from the TEM analysis of the $Co_{46}Ni_{27}Ga_{27}$ sample heat treated at 1200 °C for 4 hrs (Fig. 3.11) is that the decrease in transformation enthalpy is because of the formation of high volume fraction of γ phase in the matrix. However, in the present case, transformation enthalpies do not change in the first cycles. It can, thus, be concluded that at 350 °C, there is no γ formation.

It is obvious from the TEM analysis of the $Co_{46}Ni_{27}Ga_{27}$ sample hot rolled at 900 °C (Fig. 3.12) that γ` precipitates are very small and shifts $M_s$ to low temperatures. Therefore, the $M_s$ change, reflected in Figure 4.1, could also be because of fine γ` precipitates. Most importantly, the formation of precipitates is faster in the austenite than in the martensite. This is because of the symmetry difference of austenite and martensite crystal structures. In more symmetric crystal structures, for example in a cubic austenite, the formation of precipitates is faster than in a tetragonal martensite.

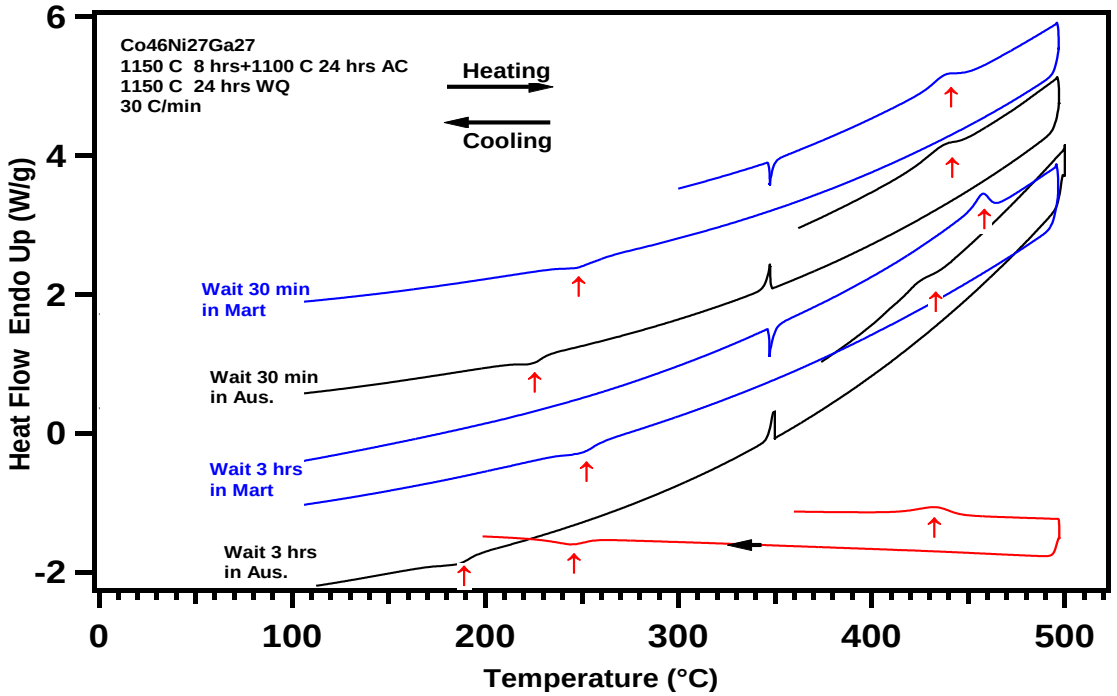


**Figure 4.1** In-situ DSC analysis of the $Co_{46}Ni_{27}Ga_{27}$ sample after initial-HT and heat treatment at 1150 °C for 24 hrs WQ, showing transformation temperature changes when the sample is aged in martensite and austenite at 350 °C for different times.

The wide exothermic peaks observed during first heating in Figures 3.5, 3.6.b and 3.7 was also observed in NiAl base alloys such as NiCoAl [61], NiMnAl [62] and NiAlFe [63] which was attributed to the ordering reaction from $L1_0$ martensite to $Ni_5Al_3$ phase. Such ordering leads to irreversibility in martensitic transformation [61, 63] and martensite stabilization manifesting itself as a the shift in $A_f$ temperature to higher levels and an increase in the transformation hysteresis [62]. In other words according to literature $Ni_5Al_3$ can completely prevent reverse martensitic transformation [61, 63] or shifts $A_f$ to high temperatures [62]. The range of the exothermic peak is 250 to 300 °C [61-63]. The transformation of $L1_0$ to $Ni_5Al_3$ occurs very rapidly in few minutes, depending on the temperature, with a diffusion controlled shear mechanism and the

structure of $Ni_5Al_3$ phase is orthorhombic $Pt_5Ga_3$ ($Ni_5Ga_3$) type structure [22]. In the present results, the exothermic peak resembles the behavior of $Ni_5Al_3$ formation from $L1_0$ matrix as described above. However $Ni_5Al_3$ prevents reverse martensitic transformation [61, 63]. In present case the wide exothermic peak has been observed in both stable (Fig. 3.7) and unstable (Fig. 3.5) cases. Therefore, it does not cause transformation irreversibility. Most importantly, it was also observed in hot-rolled sample where material is β2 austenite at that temperature (Fig. 3.6.b). If the sample heat treatment through initial-HT+1150 °C for 24 hrs (the DSC results of which shown in Fig. 3.5.a) in-situ aged in the DSC at 350 °C for 3 hrs where the wide exothermic peak is ended (Fig 3.5.a) before the reverse martensitic transformation starts, no irreversibility or change in transformation enthalpy and temperatures were observed as compared to the results shown in Figure 3.5.a. In other words, whatever process happens during the exothermic peak appearance does not continue once the exothermic peak ends. In addition, the peak only observed in the first cycles and high thermal hysteresis was observed in all cycles. Therefore the instability and high thermal hysteresis is not associated with the wide exothermic peak observed in the first cycles. It could be because of the rearrangement of point defects such as quenched-in vacancies. This mechanism is more feasible because the wide exothermic peak is observed more clearly in the samples that are fast cooled from high temperatures. When the sample (the DSC results of which presented in Fig. 3.7) is aged at RT for 2 months after the 5 DSC cycles, the wide exothermic peak is not observed again.

### 4.2. Effect of γ` Precipitation on Transformation Temperatures

Hot rolled $Co_{46}Ni_{27}Ga_{27}$ samples showed stable transformation response when the sample is cycled whether upper cycle is 230 °C which is just above the $A_f$ or 500 °C (Fig. 3.6). However, $M_s$ temperature changes with the upper cycle temperature and stay constant in the following cycles with the same upper cycle temperature (Fig. 3.6). In order to understand $M_s$ temperature change because of upper cycle temperature change, hot rolled samples aged at 500 °C and 630 °C to investigate how $M_s$ temperature changes. In addition, the transformation temperatures evolution has been recorded for the hot rolled sample upon three successive DSC cycles where upper cycle temperature is firstly 230 °C, just after the $A_f$, and then upper cycle temperature is 500 °C, and lastly again upper cycle temperature is 230 °C.

Figure 4.2 displays the forward martensitic transformation peaks of the hot rolled, hot rolled and 500 °C 3hrs, and hot rolled and 630 °C 1hr heat treated $Co_{46}Ni_{27}Ga_{27}$ samples. Reverse martensitic transformation temperatures were not shown for clarity, and most importantly, because $A_s$ and $A_f$ do not change more than 5 °C for all conditions. For hot rolled sample, three successive DSC cycles were performed and when the DSC temperature range is up to 230 °C, $M_s$ is recorded as 172 °C however when it is extended to 500 °C, the $M_s$ decreases by about 20 °C. If additional one more cycle is performed with the upper cycle temperature of 230°C, $M_s$ is recorded as 162°C. If the sample is aged at room temperature for a few days (10 days) the $M_s$ goes to first value which is 172 °C (Fig 4.2).

The decrease in $M_s$ probably originates from the formation of G-P zones like structures, which should be a precursor to γ` precipitate nuclei. The small γ` particles observed during the in-situ TEM heating-cooling in Figure 3.12 supports this hypothesis. Atomic clusters, that are precursors to γ` precipitates, start even during the DSC experiments. However, they start to disappear, even during the DSC heating and cooling across the phase transformation temperature range, indicating that martensitic transformation may be helping the dissolution of these clusters. Room temperature aging for few days is sufficient to completely dissolve these clusters, pointing out that the observed phenomenon cannot be just due to the conventional intermetallics precipitation. These clusters follow austenite matrix symmetry since they form initially in the austenite and they should form in specific lattice planes following the lattice correspondence between pre-precipitate clusters and austenite. When austenite transforms to martensite, these clusters loose lattice correspondence with the matrix, that causes driving force for diffusion. Such driving force for diffusion can lead to the dissolution of these clusters even at room temperature and help recover the reduction in the $M_s$ temperature.

After the hot rolled sample is aged at 500 °C for 3 hrs WQ same scenario is observed as in the hot rolled sample with about 10 °C $M_s$ decrease both in when up temperatures are 230 °C and 500 °C. Which means some formed γ` precipitates have taken place and caused $M_s$ decrease of 10 °C.

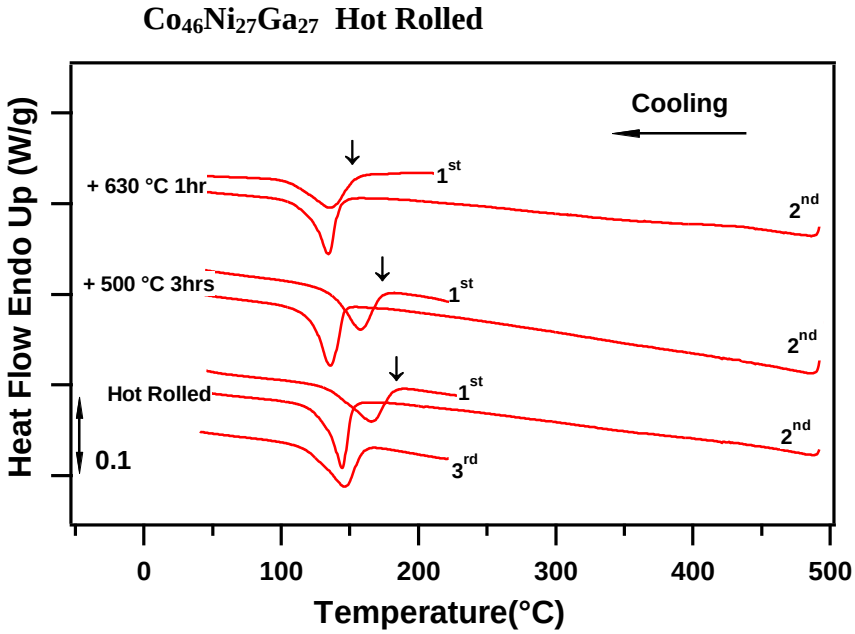


**Figure 4.2** DSC cooling curves of hot rolled and additional 500 °C for 3 hrs and 630 °C for 1hr WQ after hot rolling process $Co_{46}Ni_{27}Ga_{27}$ samples.

When the hot rolled sample is aged at 630 °C 1hr and WQ, $M_s$ was recorded as about 153 °C when the temperature range is up to 230 °C. $M_s$ decrease of 19 °C comparing to hot rolled case is because of formed γ` phase in the matrix which is also shown in TEM analysis in Figure 3.12. Formation of the fine precipitates in the matrix (Fig. 3.12.n) caused decrease in martensite twin thickness and suppressed the $M_s$ to lower temperatures. When the DSC range is extended up to 500 °C again $M_s$ decreases but this time decrease is about 8 °C which is smaller than in hot rolled sample. Again the transformation temperatures are stable after ageing at 630 °C for 1hr. To summarize, the nucleation of fine γ` phase are very rapid in hot rolled sample but the amount of

formation is limited most probably because of composition effect and does not cause continuous $M_s$ decrease.

### 4.3. Effect of γ` Precipitation on Transformation Hysteresis

Figure 4.3 shows the thermal hysteresis difference between the $Co_{46}Ni_{27}Ga_{27}$ samples with γ` and without γ` in the microstructure and thermal hysteresis versus γ phase volume fraction graph using data presented in Table 3.1 and 3.2. Figures 4.3.a-c show microstructure and martensite variant groups of $Co_{46}Ni_{27}Ga_{27}$ samples before and after hot rolling, and after hot rolling and annealing at 1000 °C followed by water quenching. Figure 4.3.d displays microstructure and martensite variant groups of $Co_{44}Ni_{26}Ga_{30}$ sample after heat treated at 900 °C for 24 hrs. Figure 4.3.e shows transformation temperatures and thermal hysteresis ($A_f$–$M_s$) for three cases as shown in Figure 4.3.a-c. Thermal hysteresis is 191 °C before hot rolling and the size of the martensite variant groups is higher than the ones after hot rolling which has 38 °C thermal hysteresis. When the hot rolled sample is annealed at 1000°C for 1 hr, most of the γ` phase particles dissolves in the matrix without any notable change in the blocky γ phase and the thermal hysteresis increase to 189 °C which is very close to that before hot rolling. Increase of $M_s$ can be explained by the change in the matrix composition after the dissolution of γ`. However, the wide thermal hysteresis can be explained by the absence of γ` which has effect on thermal hysteresis.

Without γ`, the size of martensite variant groups is dictated by the soft blocky γ phase and during transformation, they cause elastic energy dissipation which causes to wide thermal hysteresis. This is illustrated by comparing thermal hysteresis vs. γ volume

fraction in Figure 4.3.f. However, in Figure 4.3.b with γ`, the size of martensite variant groups is smaller which is dictated by hard γ` particles in the hot rolled sample and thermal hysteresis is about 38 °C even though there is a high volume fraction of γ phase (30%). In this case energy dissipation is lower and thermal hysteresis is low.

The thermal hysteresis of $Co_{44}Ni_{26}Ga_{30}$ sample heat treated at 900 °C for 24 hrs is also low about 39 °C without γ`, however, in this case, γ phase volume fraction is also low (6%) and they are small. In addition, the size of martensite variant groups is large (Fig. 4.3.d) and they are not dictated by soft and small γ phase particles which causes elastic energy dissipation during transformation. It should be noted that grain size effect on martensitic transformation characteristics is neglected in this study because in all cases grain size is higher than 100 μm. In addition, composition effect is also neglected. To summarize, high volume fraction and size of γ phase affect thermal hysteresis and the size of martensite variant groups. Wide thermal hysteresis which is because of high volume fraction of ductile γ phase can be decreased by precipitating hard γ` particles and strengthening the matrix as shown in the hot rolled case.

TEM image shown in Figure 3.12.e indicates that γ` precipitation forms preferentially near edge of the soft γ phase. Similar γ' formation has been showed in ref [43]. What is found out so far that thermal hysteresis are very sensitive to γ' precipitation which brings about a great advantage for practical applications since one can form γ' phase by low temperature heat treatments and decrease thermal hysteresis without worrying about volume fraction of soft γ phase which increases thermal hysteresis and negatively affects shape memory effect.

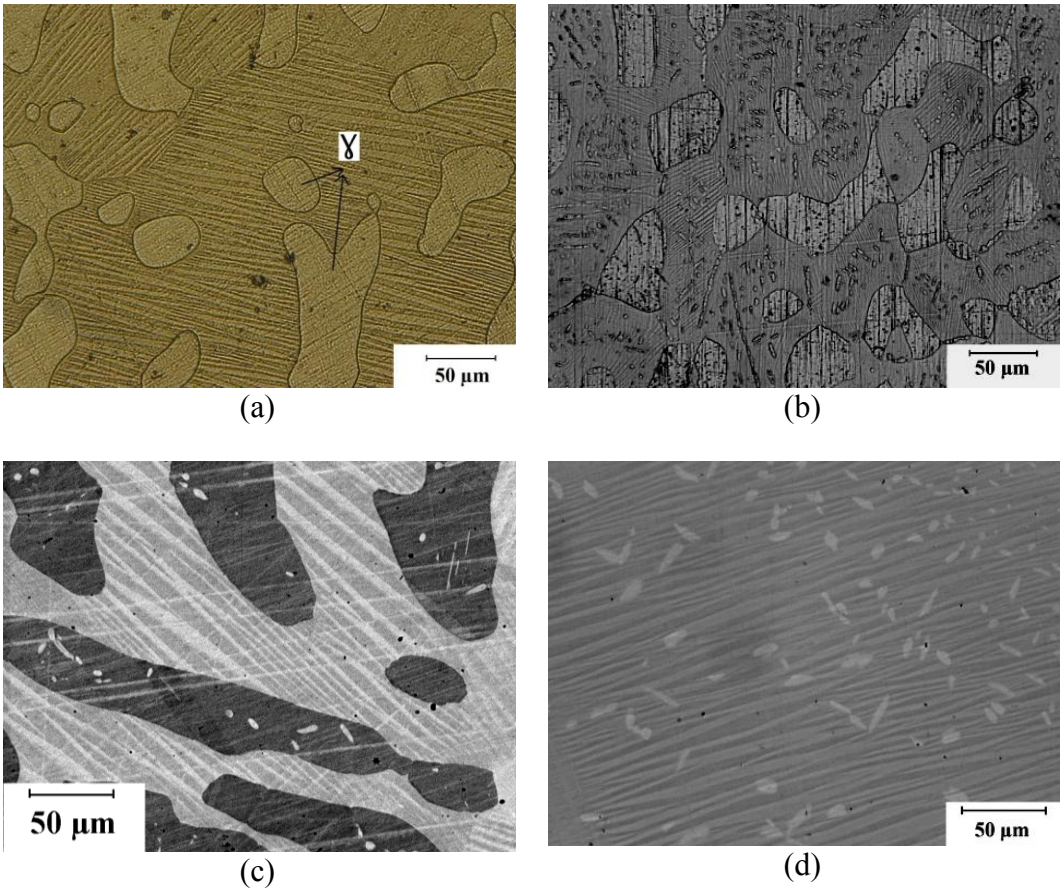


(a) (b)

(c) (d)

**Figure 4.3** Microstructure and martensite variant groups of $Co_{46}Ni_{27}Ga_{27}$ samples (a) before and (b) after hot rolling and after (c) hot rolling and annealing at 1000 °C for 1hr followed by water quenching, of (d) $Co_{44}Ni_{26}Ga_{30}$ sample after the heat treatment at 900 °C for 24 hrs. (e) Comparison of the transformation behavior of the samples in (a, c) without and in (b) with γ` phase particles. (f) Thermal hysteresis versus γ phase volume fraction for data presented in Tables 3.1 and 3.2

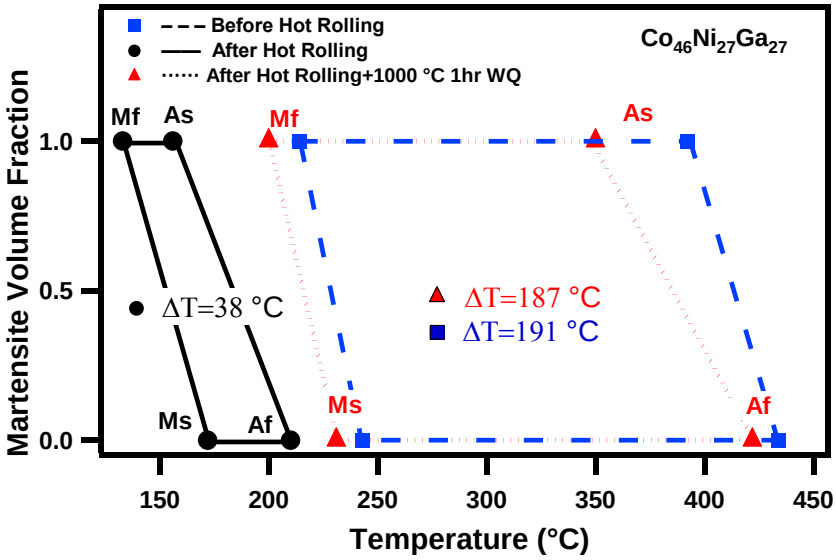


(e)

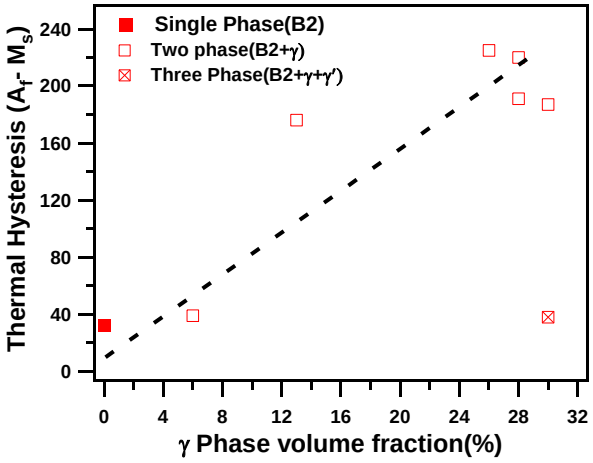


(f)

**Figure 4.3** Continued.

## 4.4 Low Temperature Aging Effect on Transformation Temperatures and Hysteresis of $Co_{44}Ni_{26}Ga_{30}$ HTSMA

Very low thermal hysteresis of 15 °C was obtained after annealing homogenized $Co_{44}Ni_{26}Ga_{30}$ sample at 300 °C for 1 hour as shown in Figure 3.15, where homogenized

sample has hysteresis of 39°C. The reason could be that is because of fine coherent γ' precipitates formed at 300 °C for 1 hour. It is well know that hard γ` precipitates increases stored elastic energy and decrease transformation hysteresis as shown in Figure 4.3.f for hot rolled $Co_{46}Ni_{27}Ga_{27}$ sample. When the sample is aged longer than 1 hour thermal hysteresis increases (Table 3.4), which is another confirmation for coherent γ` precipitation. A narrow thermal hysteresis is ideal for applications requiring fast and active control. Therefore, regarding the results, in CoNiGa alloys it is possible to decrease thermal hysteresis by low temperature ageing which is associated with γ` precipitates. However at this step, it is not clear that low temperature ageing of $Co_{44}Ni_{26}Ga_{30}$ caused γ` precipitation in the matrix although decrease of thermal hysteresis points out γ` precipitation, further experiments such as TEM is necessary.

Figure 4.4.a shows $M_s$ and thermal hysteresis versus aging temperature graph of the $Co_{44}Ni_{26}Ga_{30}$ samples for 1 hr aging time. Figure has a peak at 300 °C showing minimum transformation temperature. This graph presents only $M_s$ of the $Co_{44}Ni_{26}Ga_{30}$ single phase sample in initially homogenized condition, and the samples homogenized and aged at different low temperatures (250°C - 400°C).

In order to reveal the effect of ageing time at 300 °C on $M_s$ and thermal hysteresis, the homogenized samples have been aged for different durations as shown in Figure 4.4.b. Ageing for 1 hr gives the least thermal hysteresis.

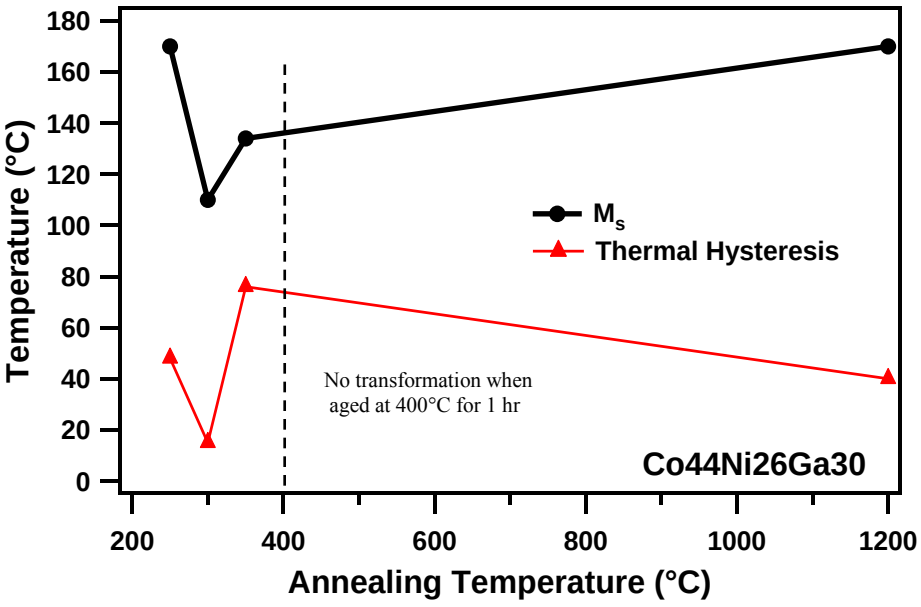


(a)

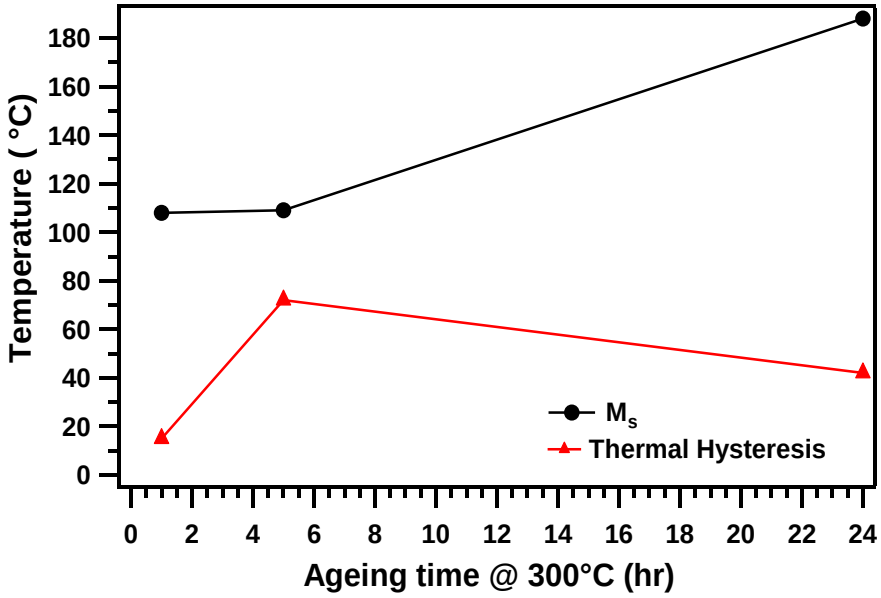


(b)

**Figure 4.4** (a) $M_s$ and thermal hysteresis versus aging temperature (250 °C-400 °C) graph of the homogenized $Co_{44}Ni_{26}Ga_{30}$ single phase samples for 1 hr aging time. (b) The $M_s$ and thermal hysteresis change with aging time at 300 °C.

### 4.5 The Effect of Valence Electron Concentration on $M_s$ Temperature

A rough linear correlation between the e/a and $M_s$ has been reported for CoNiGa SMAs in the literature [41, 44, 57]. However, other potentially important factors that influence $M_s$ are neglected. In present work, it is found that in addition to e/a, Ga content notably affects the Ms. In other words, for a constant e/a, higher Ga content results in a higher $M_s$. $M_s$ vs. e/a plot are constructed taking into account all samples with different heat treatments of $Co_xNi_yGa_z$ using DSC results and compositional analysis results from WDS measurements. Figure 4.5 presents these plots together with data from single phase $Co_xNi_yGa_z$ and $Co_xNi_yGa_z$ SMAs from the authors` earlier work and from additional study in the literature [41]. The e/a ratios were calculated using the matrix compositions measured using WDS. There is a reasonable agreement between these results and the ones reported in the literature. Oikawa *et al.* [41] reported $M_s$ vs. e/a plot for single phase CoNiGa alloys with 30 at.% Ga and 32 at.% Ga alloys which do not fall on the same line. The reason for such a difference in the Ms temperatures with different Ga contents was not rationalized. From the present results it can be concluded that $M_s$ vs. e/a relationship follows a linear trend for a constant Ga content.

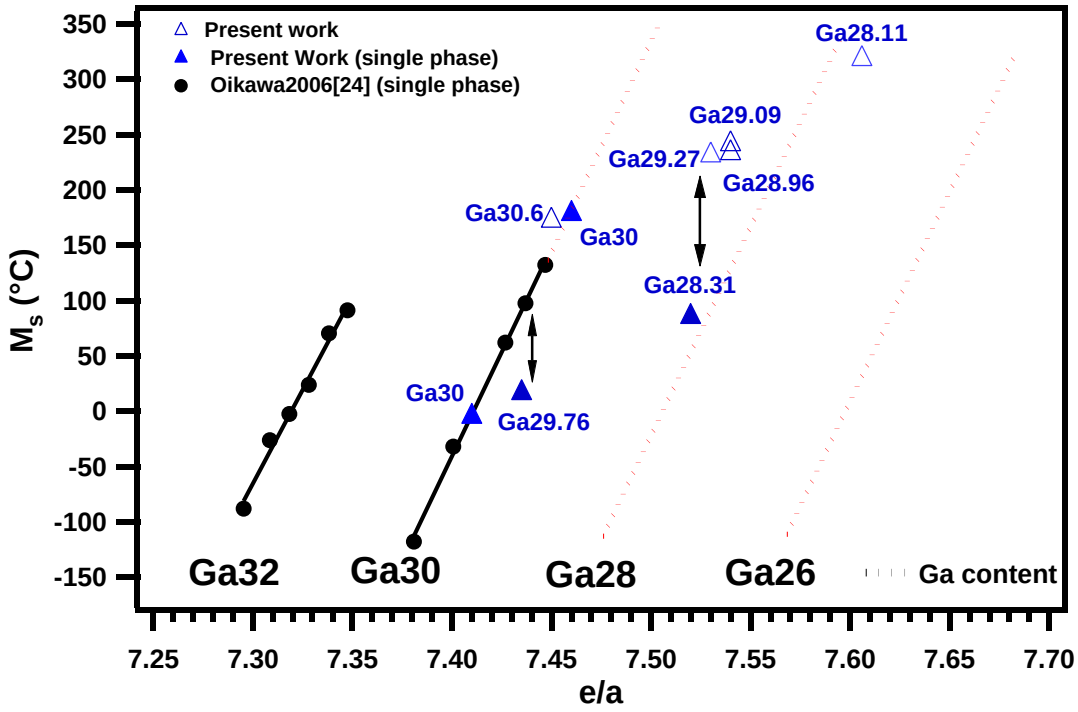


**Figure 4.5** Ms temperatures of CoNiGa SMAs with single or multiphase structures as a function of the e/a ratio and Ga content. The composition of the matrix, and thus e/a ratio, Ga content and the volume fractions of the secondary and ternary phases were altered using annealing heat treatments. Close and open symbols represents single and multiphase microstructures, respectively.

If the two lines from Oikawa *et al.*`s [41] study are extrapolated for different Ga contents, as shown by the dashed lines in Figure 4.5, it can be seen that there is a good agreement between these constant Ga content lines and the experimental data from the present work. In addition, the $M_s$ dependence on Ga content for a constant e/a ratio is obvious in Figure 4.5. For example, the e/a ratio of the two single phase samples, $Co_{46.5}Ni_{23.5}Ga_{30}$ alloy from Oikawa *et al.* [41] and $Co_{49.5}Ni_{21}Ga_{29.5}$ sample are very close and 7.346 and 7.435, respectively. However the one has higher Ga content has higher $M_s$ temperature by 80°C.

The data for single phase $Co_{44}Ni_{26}Ga_{30}$ and $Co_{49}Ni_{21}Ga_{30}$ of the present work is exactly on the 30 at. %Ga reference line, which is constructed by using data from Oikawa et al. [41]. The data points from the samples of $Co_{46}Ni_{27}Ga_{27}$ with different heat treatments lie below the proposed constant Ga lines of single phase materials. This is probably due to the different ranges of e/a ratio and the differences in the number of constitutive phases. Oikawa *et al.* [41] studied the alloy compositions with the e/a range between 7.3 and 7.45. In addition, all studied alloys had single phase.

However, in the present case, the e/a range is in between 7.45 and 7.62, and the samples have either two phase or three phase structures with various volume fractions. It is likely that in addition to the e/a ratio (of the matrix), Ga content and the presence of γ and γ' particles influence $M_s$ temperature. Additional particles in the matrix, such as soft γ phase, can cause more energy dissipation during martensite nucleation and reduction in $M_s$ for a given e/a ratio. The sample with 28.11 at.% Ga in the matrix (Table 3.1) support this argument since it does not follow the proposed constant Ga lines in the $M_s$ vs. e/a ratio figure, demonstrate lower $M_s$ than expected and it has a high volume fraction of γ phase (Table 3.1).

The reason why Ga content has a significant effect on Ms in the CoNiGa alloys are not known at this point. In NiMnGa SMAs with similar compositions, a perfect linear relationship is reported between $M_s$ and e/a ratio; regardless of the Ga content [56].

By using the data of single phase or two phase CoNiGa HTSMAs having less than 4% γ phase volume fraction, updated $M_s$ vs. e/a ratio is re-plotted in Figure 4.6. In

order to get more accurate compositions measurements, WDS analysis has been conducted on the DSC samples. The e/a ratios are calculated according to the DSC sample compositions, instead of the nominal compositions shown in the upper-left part of the graph. In addition to using the constant Ga content slopes of Oikawa *et al.* [64], 28.4 at.% Ga trend line has been added using the present results. In Figure 4.6, it can be clearly seen that for the same e/a ratio, the higher the Ga content is, the higher the $M_s$ temperature becomes.

A possible reason for the strong effect of Ga content on the $M_s$ temperature for a given e/a ratio may originate from the magnetic character of the material. The values of the magnetic valence ($Z_m$) for the constitutive elements are 1, 0, and −3 for Co, Ni, and Ga, respectively [65] . Oikawa *et al.* [41] showed a good correlation between saturation magnetization ($I_s$), curie temperature ($T_c$), and $Z_m$ of ferromagnetic SMAs. They showed that the $I_s$ and curie temperature $T_c$ increase with an increase in $Z_m$. The $Z_m$ values of the alloys having the same e/a ratio and different $M_s$ has been calculated here. The higher the $Z_m$ is, the higher the $M_s$ is observed, as shown in Figure 4.6.

Figure 4.7 displays magnetic moment vs. temperature graph of $Co_{49}Ni_{22.5}Ga_{28.5}$ and $Co_{46}Ni_{24}Ga_{30}$ alloys under 5 Tesla. These two alloys have almost the same e/a ratio but different $M_s$ temperatures (Fig. 4.6). The one has higher $M_s$ temperature, $Co_{46}Ni_{24}Ga_{30}$, has lower magnetic moment. It is likely that the $M_s$ difference in two alloys which have the same e/a ratio could originate from magnetic characteristics of the alloys. In other words, magnetic characteristics of austenite and martensite could play a

key role in the compatibility between austenite and martensite which affects $M_s$ temperature.

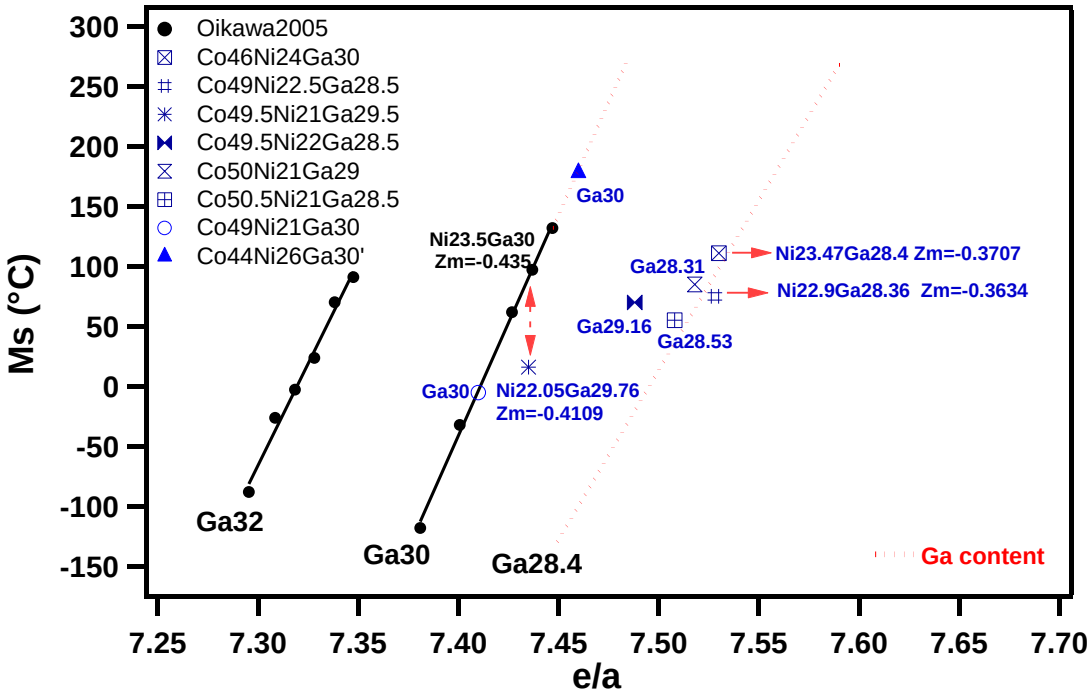


**Figure 4.6** e/a ratio and Ga content dependence of $M_s$ temperatures of CoNiGa SMAs with single or two phase structure having less than 4% γ phase volume fraction.

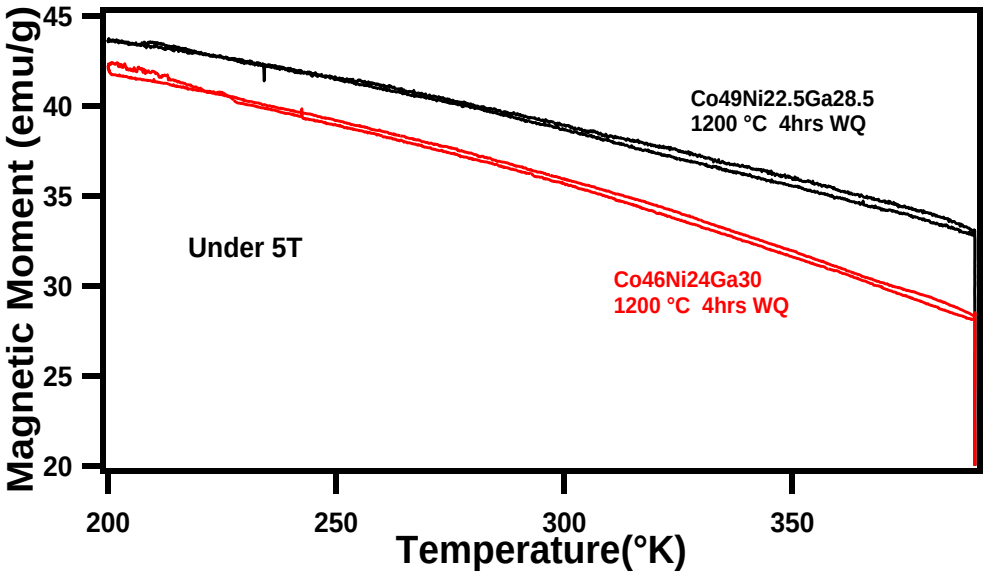


**Figure 4.7** Magnetic moment vs. temperature graph of $Co_{49}Ni_{22.5}Ga_{28.5}$ and $Co_{46}Ni_{24}Ga_{30}$ alloys under 5 Tesla.

These results show that it is possible to significantly alter $M_s$ in CoNiGa SMAs using simple heat treatments which also affect the constitutive phases and their volume fractions, and thus the composition, Ga content and the e/a ratio of the matrix. In addition, Figures 4.5 and 4.6 give a unique opportunity for CoNiGa alloy design. However, this is just a empirical finding at the best, especially in terms of the effect of Ga content. More work is underway to reveal potential physical reasons.

### 4.6 The Effects on Shape Memory Characteristics of Hot Rolled $Co_{46}Ni_{27}Ga_{27}$ HTSMA

Strain vs. temperature response of the hot rolled $Co_{46}Ni_{27}Ga_{27}$ samples along the transverse direction under various constant tension stress levels was showed in Figure 3.19. In addition, hot rolled $Co_{46}Ni_{27}Ga_{27}$ compression sample along rolling direction is

deformed at room temperature and strain recovery of the compression sample upon reverse martensitic transformation is pictured in Figure 3.20. Clearly, the transformation strain and recovery levels are pretty low which indicates either the lack of strong crystallographic texture in the austenite phase of the hot rolled sample or alternatively a strong [111] texture. Since sample $A_f$ temperature is above room temperature, texture measurement couldn't be performed which is difficult at high temperatures. In general SMAs with martensitic transformation from a cubic austenite to a tetragonal martensite, such as CoNiAl, CoNiGa, and NiMnGa SMAs, demonstrate very small transformation strain along the [111] orientation in single crystalline form [28, 37, 66-67] and recoverable strain levels are very low. The highest transformation strain is usually observed along the [100] orientation in the CoNiGa alloys [37]. Therefore, the hot rolling may have caused some level of [111] texture in the present polycrystals. Thus, it is necessary to find processing schedules to obtain nearly [100] texture for high transformation strain values in CoNiGa alloys.

The low recoverable strain values can also be a result of the high volume fraction of $\gamma$ phase which may influence the martensite variant selection under stress. This can be attributed to the relaxation of the elastic stored energy due to the presence of soft $\gamma$ phase since it may deform during martensitic transformation accommodating the transformation shear and volume change.

In the present alloy, martensitic transformation occurs between a cubic austenite phase to a tetragonal martensite phase. Greater the change in symmetry during transformation in SMAs, the greater the transformation strain will be [68]. In NiTi

SMAs which has monoclinic martensite and cubic austenite gives at least 5.5% strain recovery in polycrystalline form [68]. Low transformation strain values can also be as a result of low symmetry change during transformation of present alloy.

# CHAPTER V

# SUMMARY AND CONCLUSIONS

In this study the microstructure and martensitic transformation behavior of CoNiGa high temperature shape memory alloys have been investigated in polycrystalline form after different heat treatment conditions. In addition, the mechanical and shape memory responses have been examined for the hot rolled $Co_{46}Ni_{27}Ga_{27}$ HTSMA, which is selected for its stable transformation properties and lowest transformation hysteresis among all studies cases. Main findings and conclusions for the study can be summarized as follows:

1. There is more ductile γ phase formation observed in $Co_{46}Ni_{27}Ga_{27}$ samples than in $Co_{44}Ni_{26}Ga_{30}$. In addition, $Co_{44}Ni_{26}Ga_{30}$ alloy has a tendency to accumulate along grain boundary, while $Co_{46}Ni_{27}Ga_{27}$ does not. In addition, $Co_{46}Ni_{27}Ga_{27}$ samples failed along grain boundaries.
2. Empirical findings after thermo-mechanical process of CoNiGa HTSMAs indicate that the proportion of the γ phase volume fraction should be more than 10% in order to process successfully In addition, the effect of γ phase on ductility was clearly illustrated which prevents crack propagation.
3. Thermal cyclic instability has been observed in some $Co_{46}Ni_{27}Ga_{27}$ and $Co_{44}Ni_{26}Ga_{30}$ samples after particular heat treatments. Transformation cyclic instability in DSC analysis has been observed in some $Co_{46}Ni_{27}Ga_{27}$ samples, results from very fast γ phase precipitation formation in the matrix during

even heating for reverse transformation, which changes the matrix composition and the volume fraction of transforming phases considerably.

4. One of the most stable high temperature CoNiGa alloys with Ms of 172°C and thermal hysteresis of 38°C is obtained after hot rolling $Co_{46}Ni_{27}Ga_{27}$ alloy at 900°C with 40 % thickness reduction.
5. TEM observation revealed that γ' precipitates can be form from both β and γ regions after heating hot rolled $Co_{46}Ni_{27}Ga_{27}$ sample to 630°C. Fine γ` precipitates formed as a result of β→γ' transformation in the matrix. However massy γ` precipitates have been seen in γ region after the process of γ→γ` ordering reaction. Fine γ` precipitates, which formed in the matrix caused a decrease in $M_s$ and an increase of twin density.
6. Volume fraction and the size of γ phase affect thermal hysteresis and the size of martensite variant groups. Increasing the γ phase volume fraction causes wider thermal hysteresis. Without γ`, the size of martensite variant groups is dictated by the soft blocky γ phase, during transformation these blocky γ` precipitates cause elastic energy dissipation, which causes larger thermal hysteresis. However with γ`, the size of martensite variants groups is smaller and dictated by hard γ` particles. In this case, energy dissipation is lower, stored elastic energy is high and ,thus, thermal hysteresis is low.
7. $M_s$ temperature linearly depends on the valence electron concentration (e/a) of the matrix, only if the Ga content is constant. In other words, for a given e/a ratio, the higher the Ga content is, the higher the transformation

temperatures become. In addition, empirical results support that the volume fraction of γ phase also affects $M_s$.

8. The constant-stress thermal cycling response of the hot rolled $Co_{46}Ni_{27}Ga_{27}$ samples which have stable transformation properties were examined under incrementally increasing tensile stress levels. Low transformation strain values have been found. The low strain values can happen because of the texture effect and high volume fraction of γ which may influence the martensite variant selection under stress.

# REFERENCES


[1] Miyazaki S and Otsuka K, ISIJ International 1989; 29: 353.

[2] Tadaki T, Otsuka K, and Shimizu K, Annual Review of Materials Science 1988; 18: 25.

[3] Ma J, Karaman I, and Noebe R, International Materials Reviews 2010; In press

[4] Chang LC, Read TA, Trans. AIME 1951; 189: 47.

[5] Basinski SZ and Christian JW, Acta Metallurgica 1954; 2(1): 101.

[6] Buehler WJ, Glifrich JW, and Wiley RC, J. Appl. Phys. 1963; 34: 1475.

[7] Arbuzova IA and Khandros LG, Fiz. Met. Metalloved 1964; 17: 390.

[8] Otsuka K and Shimizu K, Scripta Metallurgica 1970; 4(6): 469.

[9] Otsuka K, Wayman CM, Nakai K, Sakamoto H, and Shimizu K, Acta Metallurgica 1976; 24(3): 207.

[10] Otsuka K, Sakamoto H, and Shimizu K, Acta Metallurgica 1979; 27(4): 585.

[11] Saburi T, Wayman CM, Takata K, and Nenno S, Acta Metallurgica 1980; 28(1): 15.

[12] Otsuka K and Wayman CM, Shape Memory Materials. London: Cambridge University Press; 1998.

[13] Duerig TW, Melton KN, Stockel D, and Wayman CM, Engineering Aspects of Shape Memory Alloys. London: Butterworth-Heinemann; 1990.

[14] Funakubo H, Shape Memory Alloys. Amsterdam: Gordon and Breach Science Publishers; 1987.

[15] Firstov GS, Van Humbeeck J, and Koval YN, Journal of Intelligent Material Systems and Structures 2006; 17(12): 1041.

[16] Van Humbeeck J, Journal of Engineering Materials and Technology 1999; 121(1): 98.

[17] Cesari E, Font J, Muntasell J, Ochin P, Pons J, and Santamarta R, Scripta Materialia 2008; 58(4): 259.

[18] Ma YQ, Jiang CB, Feng G, and Xu HB, Scripta Materialia 2003; 48(4): 365.

[19] Golberg D, Xu Y, Murakami Y, Morito S, Otsuka K, Ueki T, and Horikawa H, Intermetallics 1995; 3(1): 35.

[20] Noebe R, Gaydosh D, Ii SP, Garg A, Biles T, and Nathal M. Proceedings of SPIE 2005; 5761: 364.

[21] Tian WH, Hibino M, and Nemoto M, Intermetallics 1998; 6(2): 121.

[22] Yang JH and Wayman CM, Intermetallics 1994; 2(2): 121.

[23] Cheniti H, Bouabdallah M, and Patoor E, Journal of Alloys and Compounds 2009; 476(1-2): 420.

[24] Otsuka K and Ren X, Intermetallics 1999; 7(5): 511.

[25] Besseghini S, Villa E, and Tuissi A, Materials Science and Engineering A 1999; 273-275: 390.

[26] Meng XL, Zheng YF, Cai W, and Zhao LC, Journal of Alloys and Compounds 2004; 372(1-2): 180.

[27] Hsieh SF and Wu SK, Materials Characterization 2000; 45(2): 143.

[28] Karaca HE, Karaman I, Chumlyakov YI, Lagoudas DC, and Zhang X, Scripta Materialia 2004; 51(3): 261.

[29] Karaca HE, Karaman I, Lagoudas DC, Maier HJ, and Chumlyakov YI, Scripta Materialia 2003; 49(9): 831.

[30] Meyer D, Maier HJ, Dadda J, Karaman I, and Karaca HE, Materials Science and Engineering: A 2006; 438-440: 875.

[31] Wuttig M, Li J, and Craciunescu C, Scripta Materialia 2001; 44(10): 2393.

[32] Oikawa K, Wulff L, Iijima T, Gejima F, Ohmori T, Fujita A, Fukamichi K, Kainuma R, and Ishida K, Applied Physics Letters 2001; 79(20): 3290.

[33] Tanaka Y, Oikawa K, Sutou Y, Omori T, Kainuma R, and Ishida K, Materials Science and Engineering: A 2006; 438-440: 1054.

[34] Chernenko VA, Pons J, Cesari E, and Perekos AE, Materials Science and Engineering a-Structural Materials Properties Microstructure and Processing 2004; 378(1-2): 357.

[35] Dadda J, Canadinc D, Maier HJ, Karaman I, Karaca HE, and Chumlyakov YI, Philosophical Magazine 2007; 87(16): 2313

[36] Dadda J, Maier HJ, Karaman I, Karaca HE, and Chumlyakov YI, Scripta Materialia 2006; 55(8): 663.

[37] Dadda J, Maier HJ, Niklasch D, Karaman I, Karaca HE, and Chumlyakov YI, Metallurgical and Materials Transactions a-Physical Metallurgy and Materials Science 2008; 39A(9): 2026.

[38] Kishi Y, Craciunescu C, Sato M, Okazaki T, Furuya Y, and Wuttig M, Journal of Magnetism and Magnetic Materials 2003; 262(2): L186.

[39] Li YX, Liu HY, Meng FB, Yan LQ, Liu GD, Dai XF, Zhang M, Liu ZH, Chen JL, and Wu GH, Applied Physics Letters 2004; 84(18): 3594.

[40] Oikawa K, Ota T, Gejima F, Ohmori T, Kainuma R, and Ishida K, Materials Transactions 2001; 42(11): 2472.

[41] Oikawa K, Ota T, Imano Y, Omori T, Kainuma R, and Ishida K, Journal of Phase Equilibria and Diffusion 2006; 27(1): 75.

[42] Sato M, Okazaki T, Furuya Y, and Wuttig M, Materials Transactions 2003; 44(3): 372.

[43] Liu J, Xie H, Huo Y, Zheng H, and Li J, Journal of Alloys and Compounds 2006; 420(1-2): 145.

[44] Liu J, Xia M, Huang Y, Zheng H, and Li J, Journal of Alloys and Compounds 2006; 417(1-2): 96.

[45] Massalski TB, ASM International 1990.

[46] Dai XF, Wang HY, Liu GD, Wang YD, Duan XF, Chen JL, and Wu GH, Journal of Physics D: Applied Physics 2006(14): 2886.

[47] Chernenko VA, Pons J, Cesari E, and Zasimchuk IK, Scripta Materialia 2004; 50(2): 225.

[48] Li Y, Xin Y, Chai L, Ma Y, and Xu H, Acta Materialia 2010; 58(10): 3655.

[49] Prusik K, Morawiec H, Kostrubiec B, Prewendowski M, Dercz G, and Ziewiec K, The European Physical Journal - Special Topics 2008; 158(1): 155.

[50] Sehitoglu H, Jun J, Zhang X, Karaman I, Chumlyakov Y, Maier HJ, and Gall K, Acta Materialia 2001; 49(17): 3609.

[51] Sehitoglu H, Karaman I, Anderson R, Zhang X, Gall K, Maier HJ, and Chumlyakov Y, Acta Materialia 2000; 48(13): 3311.

[52] Ma Y, Yang S, Liu Y, and Liu X, Acta Materialia 2009; 57(11): 3232.

[53] Kireeva I, Pobedennaya Z, Chumlyakov Y, Pons J, Cesari E, and Karaman I, Technical Physics Letters 2009; 35(2): 186.

[54] Chernenko VA, Scripta Materialia 1999; 40(5): 523.

[55] Schlagel DL, Wu YL, Zhang W, and Lograsso TA, Journal of Alloys and Compounds 2000; 312(1-2): 77.

[56] Planes A, Manosa L, Acet M, ChemInform 2009; 40(47).

[57] Craciunescu C, Kishi Y, Lograsso TA, and Wuttig M, Scripta Materialia 2002; 47(4): 285.

[58] Chari A, Garay A, and Arróyave R, Calphad 2010; In Press, Corrected Proof.

[59] Ducher R, Kainuma R, and Ishida K, Journal of Alloys and Compounds 2008; 466(1-2): 208.

[60] Santamarta R, Cesari E, Muntasell J, Font J, Pons J, and Ochin P, Intermetallics 2010; 18(5): 977.

[61] Kainuma R, Ise M, Jia CC, Ohtani H, and Ishida K, Intermetallics 1996; 4(Supplement 1): S151.

[62] Kainuma R, Nakano H, and Ishida K, Metallurgical and Materials Transactions a-Physical Metallurgy and Materials Science 1996; 27(12): 4153.

[63] Kainuma R, Imano S, Ohtani H, and Ishida K, Intermetallics 1996; 4(1): 37.

[64] Oikawa K, Ota T, Imano Y, Omori T, Kainuma R, and Ishida K, Journal of Phase Equilibria and Diffusion 2006; 27(1): 75.

[65] Williams AR, Moruzzi VL, Malozemoff AP, and Terakura K, Ieee Transactions on Magnetics 1983; 19(5): 1983.

[66] Hamilton RF, Sehitoglu H, Efstathiou C, Maier HJ, Chumlyakov Y, and Zhang XY, Scripta Materialia 2005; 53(1): 131.

[67] Chumlyakov YI, Kireeva IV, Karaman I, Panchenko EY, Zakharova EG, Tverskov AV, Ovsyannikov AV, Nazarov KM, and Kirillov VA, Russian Physics Journal 2004; 47(9): 893.

[68] Bhattacharya K and Kohn RV, Acta Materialia 1996; 44(2): 529.

# VITA


| | | |
|---|---|---|
| Name | : | Ebubekir Dogan |
| Address | : | Department of Mechanical Engineering, Texas A&M University 3123 TAMU, College Station TX 77843-3123 |
| Email Address | : | ebudogan@yahoo.com |
| Education | : | B.S., Mechanical Engineering, Bogazici University, Istanbul, Turkey, 2008 |